MIT Libraries | DSpace@MIT

MIT Open Access Articles

The CH4 cycles on Pluto over seasonal and astronomical timescales

Massachusetts Institute of Technology

The CH$_4$ cycles on Pluto over seasonal and astronomical timescales

T. Bertrand [a], F. Forget [b], O.M. Umurhan [a], J.M. Moore [a],
L.A. Young [c], S. Protopapa [c], W.M. Grundy [d], B. Schmitt [e],
R.D. Dhingra [f], R.P. Binzel [g], A.M. Earle [g], D.P. Cruikshank [a],
S.A. Stern [c], H.A. Weaver [h], K. Ennico [a], C.B. Olkin [c],
the New Horizons Science Team,

[a] *National Aeronautics and Space Administration (NASA), Ames Research Center, Space Science Division, Moffett Field, CA 94035, United States*

[b] *Laboratoire de Métórologie Dynamique, IPSL, Sorbonne Universits, UPMC Univ Paris 06, CNRS, 4 place Jussieu, 75005 Paris, France.*

[c] *Southwest Research Institute, Boulder, CO 80302, United States*

[d] *Lowell Observatory, Flagstaff, AZ, United States*

[e] *Universit Grenoble Alpes, CNRS, CNES, Institut de Planétologie et Astrophysique de Grenoble, F-38000 Grenoble, France*

[f] *Department of Physics, University of Idaho 875 Perimeter Drive, Moscow, ID 83843, United States*

[g] *Department of Earth, Atmospheric, and Planetary Sciences, Massachusetts Institute of Technology, Cambridge, MA 02139, United States*

[h] *Johns Hopkins University Applied Physics Laboratory, Laurel, MD, 20723, United States*

Number of pages: 47
Number of tables: 2
Number of figures: 18

Proposed Running Head:

Please send Editorial Correspondence to:
Tanguy Bertrand
National Aeronautics and Space Administration (NASA), Ames Research Center, Space Science Division, Moffett Field, CA 94035, United States

Email: tanguy.bertrand@nasa.gov

ABSTRACT

Pluto's surface is covered in numerous CH_4 ice deposits, that vary in texture and brightness, as revealed by the New Horizons spacecraft as it flew by Pluto in July 2015. These observations suggest that CH_4 on Pluto has a complex history, involving reservoirs of different composition, thickness and stability controlled by volatile processes occurring on different timescales. In order to interpret these observations, we use a Pluto volatile transport model able to simulate the cycles of N_2 and CH_4 ices over millions of years. By assuming fixed solid mixing ratios, we explore how changes in surface albedos, emissivities and thermal inertias impact volatile transport. This work is therefore a direct and natural continuation of the work by Bertrand et al. (2018), which only explored the N_2 cycles. Results show that bright CH_4 deposits can create cold traps for N_2 ice outside Sputnik Planitia, leading to a strong coupling between the N_2 and CH_4 cycles. Depending on the assumed albedo for CH_4 ice, the model predicts CH_4 ice accumulation (1) at the same equatorial latitudes where the Bladed Terrain Deposits are observed, supporting the idea that these CH_4-rich deposits are massive and perennial, or (2) at mid-latitudes (25°-70°), forming a thick mantle which is consistent with New Horizons observations. In our simulations, both CH_4 ice reservoirs are not in an equilibrium state and either one can dominate the other over long timescales, depending on the assumptions made for the CH_4 albedo. This suggests that long-term volatile transport exists between the observed reservoirs. The model also reproduces the formation of N_2 deposits at mid-latitudes and in the equatorial depressions surrounding the Bladed Terrain Deposits, as observed by New Horizons. At the poles, only seasonal CH_4 and N_2 deposits are obtained in Pluto's current orbital configuration. Finally, we show that Pluto's atmosphere always contained, over the last astronomical cycles, enough gaseous CH_4 to absorb most of the incoming Lyman-α flux.

1 Introduction

1.1 *Pluto's ices as observed by New Horizons in 2015*

In July 2015, our vision of Pluto changed as the New Horizons spacecraft revealed a frozen world with unprecedented landscapes in the Solar System (Stern et al., 2015). The first analysis of spectral data from the Linear Etalon Imaging Spectral Array (LEISA) instrument on-board New Horizons showed that Pluto's water ice bedrock is covered by volatile ices such as N_2, CH_4 and CO, except in some parts of the equatorial regions, covered only by dark tholins (Grundy et al., 2016). Detailed spectroscopic analysis then revealed a more complex volatile ice distribution with different types of ice mixtures on Pluto's surface (Schmitt et al., 2017; Protopapa et al., 2017).

The exact nature of the observed deposits is not easy to derive from these spectroscopic analyses, because they involve many parameters such as the abundance, dilution state, texture, or grain size, which are poorly constrained (Schmitt et al., 2017). A first extraction of these parameters at the global scale is solved through sophisticated inversion of a Hapke's radiative transfer model of the LEISA data (Protopapa et al., 2017). However, spectroscopic analyses of the surface do not provide information about the thickness of these deposits. The thickness can be inferred from geological insights using high resolution images from the LOng-Range Reconnaissance Imager (LORRI) instrument and albedo maps, that help distinguish a thin frost of ice from a massive deposit. A simplified global picture of the volatile ice reservoirs on Pluto is shown in Figure 1.

The most prominent volatile ice deposit on Pluto's surface is a kilometer-thick ice sheet made of N_2 ice, mixed with CH_4 and CO, which is sequestered in Sputnik Planitia[1], the vast topographic basin at the anti-Charon longitude (Stern et al., 2015; Grundy et al., 2016). This perennial glacier is the main reservoir of N_2 ice.

Methane is detected almost everywhere in the northern hemisphere, with varying brightness, textures and mixtures (such as CH_4-rich ice and CH_4 diluted in N_2-rich ice), as highlighted in the available maps of the equivalent width of absorption in the Multi-spectral Visible Imaging Camera (MVIC) CH_4 filter (Grundy et al., 2016; Earle et al., 2018b) as well as in LEISA maps (Protopapa et al., 2017; Schmitt et al., 2017).

The North Pole is covered by relatively pure and bright CH_4-rich ice, with an

---

[1] The place names mentioned in this paper include a mix of officially approved names and informal names.

estimated Bond albedo higher than 0.7 (Buratti et al., 2017).

The mid-latitudes plains (25°N-70°N) are covered in mixtures of N_2-rich and CH_4-rich ices following a latitudinal trend (Schmitt et al., 2017; Protopapa et al., 2017; Earle et al., 2018b). The latitudes 55°N-70°N are enriched in CH_4, with few N_2-rich deposits mostly confined in the depressions. The latitudes 35°N-55°N are dominated by N_2-rich ices, while the latitudes 25°N-35°N are covered again mainly of CH_4-rich ices Protopapa et al. (2017). Interestingly, the CH_4-rich deposits in these regions seem to form a relatively thick mantle, maybe 100-1000 m, given the fact that they cover some craters and give to the surface a smooth aspect.

The equatorial regions (25°S-25°N) show a greater diversity of terrains in longitude, in terms of albedo (Buratti et al., 2017), color (Olkin et al., 2017) and composition (Schmitt et al., 2017). Outside Sputnik Planitia, in the region of Tartarus Dorsa (East of Tombaugh Regio, 5°S-28°N), relatively pure CH_4-rich ice has been detected in the Bladed Terrain Deposits (BTD, Moore et al., 2018; Schmitt et al., 2017; Protopapa et al., 2017; Earle et al., 2018b). These terrains are characterized by parallel sets of steep ridges and sharp crests and are situated on high ground (above 2 km), which may indicate very massive CH_4-rich deposits, at least 300 m thick (Moore et al., 2018). They are relatively dark, with an estimated Bond albedo between 0.5-0.6 (Buratti et al., 2017). Their distinctive texture on Pluto's maps suggests that they extend further east, from longitudes 210°E to 40°E, and further south, down to 25°S (see Fig. 3 in Olkin et al., 2017; Moore et al., 2018). They also seem to be interspersed with N_2-rich flat-floored bright plains located in the depressions and valleys of these regions.

Finally, the eastern part of Tombaugh Regio (between Sputnik Planitia and Tartarus Dorsa) is bright and also contains N_2-rich and CH_4-rich ices with N_2 mostly detected in the depressions (Schmitt et al., 2017; Protopapa et al., 2017).

These observations raise the following questions: What drives the observed ice distribution and the diversity of N_2-rich and CH_4-rich terrains? Are these reservoirs perennial (lasting for many Pluto years, e.g. glaciers) or seasonal (disappearing over one Pluto year, e.g. frosts)? How do they evolve over astronomical and seasonal timescales? In this paper, we aim to provide answers to these questions by simulating the long-term evolution of N_2 and CH_4 ice, using the Pluto volatile transport model developed at the Laboratoire de Météorologie Dynamique (LMD, Bertrand and Forget, 2016; Bertrand et al., 2018).
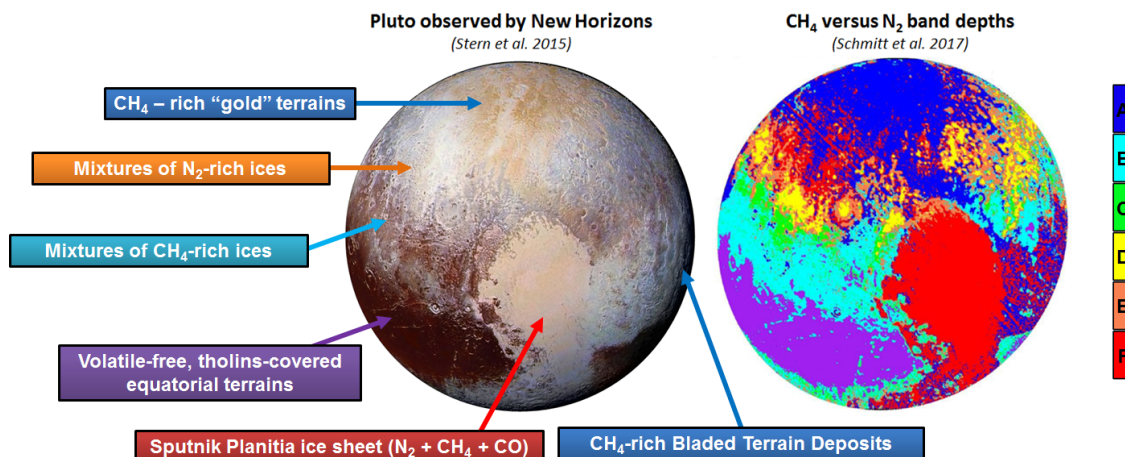
Fig. 1. The different types of terrains observed on Pluto (left) and the associated N_2-CH_4 mixtures (right). The color scale is described in details in (Schmitt et al., 2017): **A-B** relatively pure CH_4 ice, or N_2-rich ice with grains $<$ few cm and CH_4 $> 1\%$. **D-E** large N_2-rich grains (> 10 cm) with small amount of CH_4 (0.1-1%). **C** N_2-rich ice with both medium N_2 grain size ($<$ few cm) and $CH_4 < 1\%$. **F** very large N_2 ice grains (> 20 cm) with $CH_4 > 1\%$.

1.2 Modeling of volatile transport on Pluto

Global volatile transport models of Pluto have been used to explain how changes in insolation over the course of Pluto's orbit affect the surface and subsurface temperatures (which plays a key role in the Pluto environment), resulting in latitudinal variations of distribution of volatile ices (Young, 1993; Hansen and Paige, 1996; Spencer et al., 1997; Young, 2012, 2013; Hansen et al., 2015; Toigo et al., 2015; Olkin et al., 2015; Bertrand and Forget, 2016; Bertrand et al., 2018).

In particular, Bertrand and Forget (2016) (hereinafter referred as BF2016) simulated the transport of N_2, CH_4 and CO ices over tens of thousands Earth years and obtained a seasonal cycle that reproduces, to first order, the ices distribution observed by New Horizons in 2015. They showed that N_2 ice inevitably accumulates inside Sputnik Planitia basin, because of an atmosphere-topography process: the N_2 surface pressure and condensing temperature are higher at the bottom of the basin than outside, and therefore the N_2 deposits in the basin are warmer and loose more energy by thermal infrared cooling, which is balanced by a stronger N_2 condensation at that location (so that enough latent heat is released to ensure that the surface remains at the equilibrium temperature). In their simulations, the equatorial regions (apart from Sputnik Planitia) always remained warmer than at least one of the two poles (at any given time) and therefore no volatile condensed there, which explained

the dark equatorial band of Pluto. They also showed that the lower volatility of CH_4 ice at Pluto's surface temperatures allows it to exist elsewhere than in the Sputnik Planitia ice sheet, forming frost even at locations where N_2 ice would immediately sublime. In their model, CH_4 ice seasonally covered both hemispheres, and, if its albedo was high enough, N_2 was able to condense on it and form a latitudinal band around 45°N in 2015, in agreement with New Horizons observations (Figure 1). This impact of the ice albedo is also highlighted by Earle et al. (2018a), who suggest that runaway albedo variations are more efficient in the equatorial regions than at the poles, forming stark contrasts in albedo and volatile abundance.

However, the simulations performed in BF2016, and in most previous volatile transport modeling studies on Pluto, had two main limitations. First, they only considered small amounts of ice and were therefore not able to reproduce the formation of perennial glaciers. For instance, the globally averaged volatile ice reservoir used in BF2016 is only of few millimeters, in order to reach a steady state over the annual timescale. Secondly, they only focused on the 10^4 Earth years timescales, with the present orbital and obliquity parameters. Yet Pluto's high obliquity (currently around 119.6°) varies by about 23° over a period of 2.8 millions of Earth years (2.8 Myrs herein refers to the astronomical timescale) while Pluto's longitude of perihelion regresses by 360° over 3.7 Myrs (Dobrovolskis et al., 1997; Spencer et al., 1997). Both parameters impact the duration and intensity of the seasons, and the latitudes where volatile ices accumulate (Binzel et al., 2017; Earle et al., 2017).

Recently, Bertrand et al. (2018) (hereinafter referred as B2018) improved the Pluto volatile transport model described in BF2016 by implementing the most recent topography data of Pluto, the variations of obliquity, longitude of perihelion and eccentricity with time, and by taking into account a realistic N_2 reservoir as well as a N_2 ice viscous flow model. Thanks to this modeling effort, they explored the cycles of N_2 over several astronomical cycles (up to 30 Myrs). Their results explained many geological features of Sputnik Planitia, such as the evidence of recent and past glacial flow and erosion, the presence of sublimation pits in the southern portion of the ice sheet, as well as the brightness and composition of the surface ice. They also showed that large N_2 ice deposits can remain relatively stable and persist over tens of millions of years in the equatorial regions or over mid-latitudinal bands, in particular at low elevations.

1.3   Objectives of this paper

In this paper, we want to carry this work forward and explore the CH_4 cycles over astronomical and seasonal timescales with the latest version of the Pluto

volatile transport model. In particular, our objectives are:

(1) To determine the latitudes where CH_4 ice tends to accumulate over millions of years.
(2) To investigate how the CH_4 albedo impacts the N_2 condensation-sublimation cycles and the latitudinal ices distribution.
(3) To compare our results with New Horizons observations of Pluto's surface (e.g. Stern et al., 2015; Grundy et al., 2016; Moore et al., 2016), explain the observed latitudinal distribution of volatile ices (Schmitt et al., 2017; Protopapa et al., 2017), infer the nature (perennial or seasonal) of the observed deposits, and discuss the possible scenarios for their formation.

To fulfill these objectives, we adapt the Pluto volatile transport model described in B2018 so that it also takes into account the CH_4 cycle. In Section 2, we detail the recent model improvements, the assumptions made and the simulation settings. The results are presented in two independent sections. We first perform simulations with a global uniform CH_4 ice albedo (Section 3). Then, we perform simulations with two CH_4 albedo values (Section 4) depending on the latitude of the deposit, with a low value in the equatorial regions (old dark deposits) and high values in the mid-to-polar regions (bright deposits, above 30°). Our results are summarized in Table 2, and discussed in Section 5.

2   The Pluto volatile transport model

We use the latest version of the LMD Pluto volatile transport model, as described in BF2016, B2018 and Forget et al. (2017). The model settings are similar to those in B2018 except for the following changes, summarized in Table 1.

2.1   General settings of the simulations

The simulations of this paper are performed on a horizontal grid of 32×24 points, which corresponds to a grid-point spacing of 7.5° in latitude by 11.25° in longitude (about 150 km at the equator). We perform simulations over 30 Myrs using the paleoclimate mode, the N_2 ice viscous flow scheme and the ice equilibration algorithm described in details in B2018: the model is run over 5 Pluto years, then the annual mean ice rate of the last Pluto year is used to estimate the new amounts of ice over a paleo-timestep Δt and finally the topography is updated according to the new amounts of ice and the orbital parameters and the obliquity of Pluto are changed according to the new epoch $t+\Delta t$. The maximal change of obliquity within Δt must remains lower than

8

the latitudinal resolution used. Here we use $\Delta t = 100{,}000$ Earth years, that is about 400 Pluto orbits, allowing fast computing times and reasonable time resolution, with a maximal change of obliquity within that timeframe of about 3° (Binzel et al., 2017).

Most of the atmospheric effects are neglected in the model (clouds, radiative effect of the atmsphere...). As in BF2016, volatile transport occurs through the atmosphere via a parametrization of the atmospheric circulation, using a characteristic timescale $\tau_{CH4} = 10^7$ s (about four terrestrial months) to globally mix gaseous CH_4.

Paleo-timestep	$\Delta t = 100{,}000$ Earth years
Reservoirs (global average)	$R_{N_2} = 300$ m [a]
	$R_{CH_4} = 4$ m [b]
Albedo	$A_{N_2} = 0.7$
	$A_{CH_4} = 0.5\text{-}0.8$
	$A_{bedrock} = 0.1$
Emissivity	$\varepsilon_{N_2} = 0.8$
	$\varepsilon_{CH_4} = 0.8$
	$\varepsilon_{bedrock} = 1$
Thermal inertia	TI = 400-1500 SI [c]
Atmospheric mixing timescale	$\tau_{N_2} = 1$ s
	$\tau_{CH_4} = 10^7$ s
CH_4 ice mixing ratio in N_2	0.5 %

[a] *Fills Sputnik Planitia up to 2500 m below the mean surface level*

[b] *In Section 4, an infinite reservoir is used*

[c] *SI = $J\ s^{-0.5}\ m^{-2}\ K^{-1}$*

Table 1

Settings and surface conditions assumed in our simulations. In this work we assess the impact of subsurface thermal inertia and CH_4 ice albedo.

2.2 Assumptions on the state of N_2 and CH_4 ice in the model

On Pluto, CH_4 and N_2 easily mix together and are not expected to exist in perfectly pure state (Trafton, 2015; Tan and Kargel, 2018). Analysis of the New Horizons LEISA spectral observations of Pluto's surface has been performed using sophisticated spectral models and reveal complex mixtures in different amounts, also involving CO and contamination by tholins (Grundy et al., 2016; Protopapa et al., 2017; Schmitt et al., 2017). Most of the volatile ice covering Pluto's surface seems to be dominated by N_2-rich:CH_4 (e.g. Sputnik Planitia) or CH_4-rich:N_2 (e.g. the north pole). Observations also suggest mixtures of both N_2-rich + CH_4-rich at some locations, but the exact nature of these deposits is uncertain for now because they could fall into three distinct possible categories: (1) intimate mixture or intermolecular mutual attraction, at the grain scale, (2) geographic mixtures (N_2-rich + CH_4-rich could be observed at the pixel scale but not be mixed, striclty speaking, as they could be spatially disconnected at smaller scales), (3) stratification (a thin layer of CH_4-rich ice could form at the top of a N_2-rich deposit).

The scenario of intimate mixtures suggests a perfect thermodynamic equilibrium of two types of cristals at significant depth, strickly following the binary phase diagram. This is typical of instantaneous thermodynamic equilibrium but should not apply to Pluto, which we believe is a non-equilibrium dynamical environment with continuous exchange of materials. Instead, CH_4-rich and N_2-rich ices may co-exist because of dynamical processes such as sublimation, which would lead to stratification (N_2 sublimation leaving CH_4 behind and leading to a CH_4-rich ice layer on top of the N_2-rich ice).

However, the mechanisms controlling the formation and evolution of such N_2-rich + CH_4-rich mixtures remain largely unknown. With regards to this, the model presented in this paper is rather simple. As in BF2016, it does not compute any evolution of ice mixing ratio. In the simulations, the surface is either volatile-free, covered by pure CH_4 ice or by N_2-rich:CH_4 ice. Pure CH_4 ice is an approximation for unsaturated CH_4-rich ice. We make the approximation that such a CH_4-rich ice behaves almost like pure CH_4 ice, in terms of temperature and vapor pressure at saturation of CH_4. It can form after sublimation of N_2 ice (in which it was trapped before) or directly on a volatile-free surface (its lower volatility than N_2 allows it to condense where N_2 would instantly sublime). For instance, CH_4-rich ice has been observed on top of mountains in the region of Chtulhu, where N_2 could not have condensed at first (because of the significantly high altitude and low albedo of these terrains).

When both CH_4 and N_2 ices are present on the surface, we assume that CH_4 is diluted in a solid solution N_2:CH_4 with 0.5% of CH_4, as retrieved from telescopic observations (Merlin, 2015) and overall from the New horizons LEISA spectroscopic data (see spectra g and j in Table 3 in Protopapa et al., 2017). This modeled N_2-rich:CH_4 ice sublimes by conserving the 0.5% of diluted CH_4. In the next sections of this paper, we refer to this phase as N_2 ice.

The impact of N_2-rich + CH_4-rich mixtures is out of the scope of this paper, and we neglect their effect in the model. By doing so, we assume that this state corresponds to a short transient phase. In the future, we plan to investigate further stratification mechanisms and implement them in the volatile transport model. To do this, experimental studies of these processes are also strongly needed.

2.3   Surface properties

As in B2018, we use a reference N_2 ice albedo and emissivity which remain fixed to 0.7 and 0.8 respectively. The surface N_2 pressure simulated in the model is constrained by these values. The albedo and emissivity of the bare ground (volatile-free surface) are set to 0.1 and 1 respectively, which corresponds to

a terrain covered by dark tholins such as Cthulhu. CH_4 ice emissivity is fixed to 0.8 in all simulations, but we explore different values of CH_4 ice albedo, ranging from 0.3 to 0.8 depending on the simulation (the reference albedo is 0.5). Note that CO is also transported by the model, but plays no role, as we assume it always "follows" N_2.

The reference seasonal thermal inertia (TI) of the subsurface is uniformly set to 800 SI, as in B2018. However we also performed simulations using a uniform soil TI set to 400 or 1200 SI (Section 3.3), and simulations in which each type of terrain (water ice bedrock, N_2 or CH_4 ice) has its own TI ranging from 400 to 1200 SI (see Table 2 and Section 4.6).

We also tested some scenarios in which the N_2 ice surface emissivity depends on its temperature and crystalline phase (e.g. simulation #TI888_050_065_phase). We assumed a minimal emissivity of ε_α=0.3 when the ice is in its α-phase, with a surface temperature T_s below the transition temperature of $T_{\alpha-\beta}$=35.6 K and a maximal emissivity of ε_β=0.8 in its β-phase, based on the results from Stansberry and Yelle (1999). We use a simple hyperbolic tangent function for the transition:

$$\varepsilon_{N_2} = \frac{1}{2}\left[1 + tanh(\ 3\ (T_{\alpha-\beta} - T_s)\ )\right]\ (\varepsilon_\alpha - \varepsilon_\beta) + \varepsilon_\alpha \qquad (1)$$

As predicted by Stansberry and Yelle (1999), the N_2 ice surface temperature in these simulations remains at the transition temperature of 35.6 K during most of Pluto's northern fall and winter, because the emissivity change leads to a negative feedback of surface temperatures. The exchange of latent heat between both phases also leads to a negative feedback and plays a role in locking the temperature to the transition, but here we neglect this effect for sake of simplicity. Note that the α-phase of N_2 ice has never been observed in the outer solar system. Here we only test the case of an extremely low emissivity for N_2 ice in α-phase, which enables us to assess the maximum possible effect of this change on Pluto's climate.

2.4 Reservoirs

All simulations are run with N_2 ice initially placed in Sputnik Planitia in a ~10 km deep elliptical basin, as described in B2018. N_2 ice fills this modeled basin up to 2.5 km below the mean surface level, which corresponds to a global N_2 reservoir of ~300 m. N_2 is allowed to condense and sublime everywhere on Pluto's surface, depending on the computed local surface thermal balance.

The simulations performed with a uniform CH_4 ice albedo (Section 3) use a global CH_4 reservoir of 2000 $kg\,m^{-2}$, which corresponds to 4 m, if we assume

a CH_4 ice density of 500 $kg\,m^{-3}$ (Leyrat et al., 2016). This amount is low compared to the total reservoir of CH_4 ice expected on Pluto. Indeed, the BTD only could correspond to a reservoir of 22 m on global average if we assume that they cover an equatorial surface equivalent to 10° in latitudes and 180° in longitudes and that they are only 500 m thick. This is a lower limit for CH_4 ice, since the BTD may be thicker and since other km-thick reservoirs may exist in the mid-latitudinal regions. However, running simulations with such a CH_4 ice reservoir is challenging, because the CH_4 condensation-sublimation rates are very low. Typically, one meter of CH_4 ice evolves over one million years. Therefore the total amount of CH_4 ice in our simulations is a trade-off between having the largest possible reservoir and reaching a steady state for ice distribution within tens of Myrs.

Alternatively, the simulations performed with a dual CH_4 ice albedo (Section 4) are initialized with an infinite source of CH_4 ice at the location of the observed BTD in the equatorial regions.

2.5 Other settings related to the CH_4 cycle

The model does not allow CH_4 ice to flow and the topography does not change according to the accumulation or loss of CH_4 ice (it only changes according to the variation of N_2 ice thickness). These choices are driven by the fact that (1) the CH_4 reservoir involved in the model is relatively low (see above) and (2) the CH_4 ice may be too rigid to lead to a significant glacial flow activity (Eluszkiewicz and Stevenson, 1990; Moore et al., 2017, 2018), as suggested by the steep slopes of the BTD's ridges (20°), which is also why these terrains are described as massive deposits instead of glaciers.

Finally, for the simulations performed with a uniform CH_4 ice albedo (Section 3), we prohibit CH_4 to condense in the Sputnik Planitia N_2 ice sheet (we do not allow any CH_4 in SP). By doing this, we prevent the entire CH_4 reservoir to be trapped in Sputnik Planitia after several Myrs and we always conserve the same mass of CH_4 ice outside the basin. On Pluto, mechanisms or other sources must exist to maintain a certain amount of CH_4 ice outside Sputnik Planitia (see Discussions in Section 5). For instance, saturation of N_2-rich ice with CH_4, or formation of a CH_4-rich layer on top of N_2-rich ice are processes that could limit further condensation of CH_4 in SP, and maintain significant amounts of CH_4 ice outside SP.

3 Simulations with a uniform CH_4 ice albedo

In this section we investigate where CH_4 ice tends to accumulate over astronomical timescales.

3.1 Initial state of the simulation

The simulations are performed using the New Horizons topography data, starting with all N_2 ice filling a deep modeled Sputnik Planitia basin up to 2.5 km below the mean surface level, and with a 4-meter thick layer of CH_4 ice covering the entire globe. The simulation is performed with a unique albedo for CH_4 ice, set to 0.5, and a uniform thermal inertia of 800 SI. We then let the volatile ices evolve over 30 Myrs.

3.2 Results: formation of massive equatorial deposits and mid-to-polar frosts of CH_4

Figure 2 shows the evolution of the CH_4 ice distribution obtained over the last 30 Myrs. The ice quickly accumulates in the equatorial regions. Typically, after 10 Myrs, 20-40 m thick CH_4 deposits ($1\text{-}2\times10^4$ kg m^{-2}) are formed between 12°S-22.5°N (by accumulation of the CH_4 ice which was initially placed at the poles). The maximal net rates of sublimation are obtained at the poles. Above 30° latitude, 4 meters of ice can disappear within one astronomical cycle (2.8 Myrs). By extrapolation, if we had started with a global CH_4 ice reservoir of 100 m, we would have obtained ~ 1 km thick deposits in the equatorial regions after 50-100 Myrs.

Why is CH_4 ice accumulating at the equator? Because of Pluto's high obliquity, ranging from 104° to 127° over 2.8 Myrs, the polar regions receive more solar flux than the equator on average. If one assumes medium to large soil thermal inertia, this leads to colder equatorial regions on average over several Myrs (see Fig. 4.B in B2018). In addition to the obliquity cycle, Pluto's solar longitude of perihelion (L_{speri}) oscillates over a period of 3.7 Myrs and leads to asymmetries in the seasons (Dobrovolskis et al., 1997; Binzel et al., 2017). For instance, when Pluto's L_{speri} is close to 90°, the northern polar latitudes undergoes a short and intense summer (close to the perihelion) and a long and intense winter (close to the aphelion) while the southern polar latitudes undergoes a long summer far from the sun and a short winter close to the sun, and vice versa when the orbital conditions are reversed (L_{speri} close to 270°). As a result, the northern hemisphere tends to be colder on annual average when
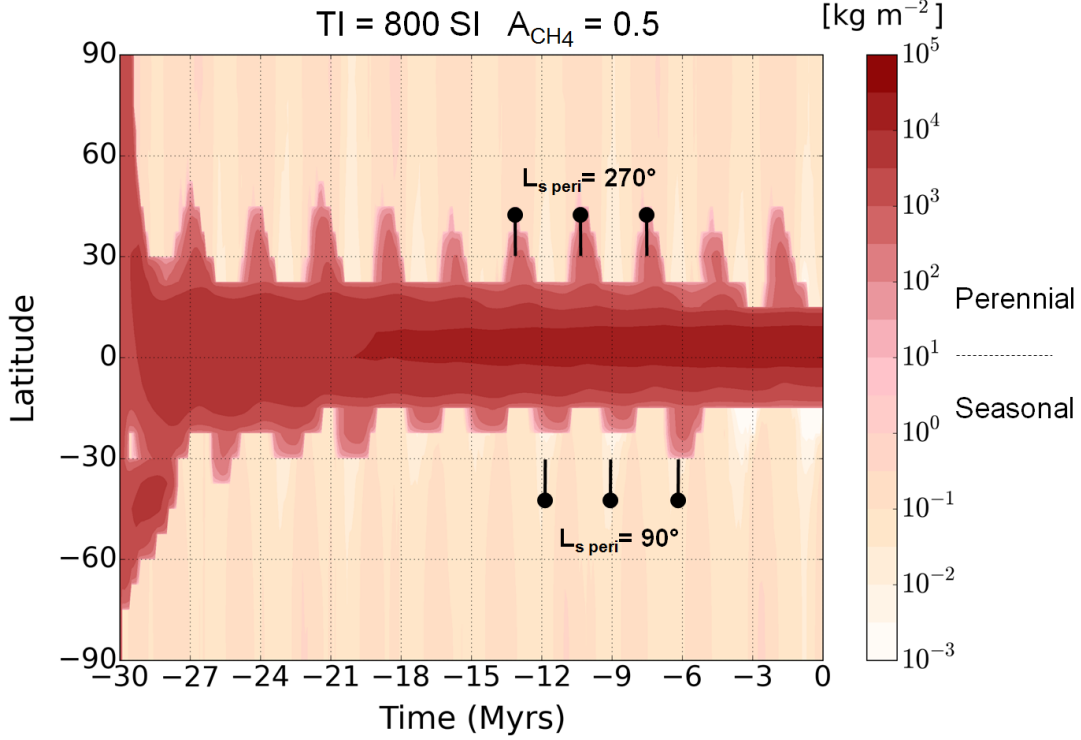
Fig. 2. Evolution over 30 Myrs of the perennial and seasonal deposits of CH_4 ice on Pluto in our simulation with a unique CH_4 ice albedo of 0.5 (the values shown correspond to the zonal annual mean amount of CH_4 ice in $kg\,m^{-2}$, for the areas outside of Sputnik Planitia). CH_4 ice quickly accumulates in the equatorial regions, where it forms massive deposits. At higher latitudes, only thin seasonal CH_4 deposits form. The black vertical lines indicate the periods where L_{speri} is close to 90° and 270° (when seasonal asymmetries are the strongest).

Pluto's L_{speri} is close to 90°, and warmer when Pluto's L_{speri} is close to 270° (see Fig. 4.A in B2018).

However, our results show that when L_{speri} is close to 90°, the intense northern summer (occurring close to the perihelion) removes a significant amount of CH_4 ice at the north pole and during this epoch CH_4 ice accumulates at the equator and in the southern hemisphere. Conversely, when L_{speri} is close to 270°, CH_4 accumulates at the equator and in the northern hemisphere. This is illustrated by Figure 2 showing that CH_4 deposits extend to higher latitudes (20°S and 45°N) during the periods of asymmetric seasons (L_{speri} close to 90° or 270°).

On average over one astronomical cycle, the equatorial regions are a net accumulation zone of CH_4 ice, while the poles are a net sublimation zone. This result is consistent with New Horizons observations of the CH_4-rich BTD in the equatorial regions (Moore et al., 2016, 2018) and supports the fact that they are thick and perennial CH_4 deposits.

Figure 2 also shows that the modeled CH_4 deposits are not symmetric to the equator, as they tend to be more extended to the northern latitudes, in accordance with the observed latitudinal extent of the BTD (5°S-25°N). This is because during the last 70 Myrs, the L_{speri} value at high obliquity remained close to 90° and led to an asymmetry of insolation and surface temperatures which favors a slightly warmer south hemisphere (see details and Fig. 5 in B2018, and Discussions in Section 5).

Note that our modeling does not reproduce the bladed aspect of the BTD nor explain why they are mostly located in the eastern hemisphere, although it may be due to the fact that the dark tholin-covered surface in the western hemisphere (Cthulhu) prevents condensation of CH_4 (assuming that the BTD formed after Cthulhu). It is likely that this longitudinal asymmetry has dynamical origins and therefore it should be investigated by using 3D global climate models (which include a full 3D dynamical core).

Although thick deposits of CH_4 ice are not stable at the poles, thin CH_4 frost (< 1 mm) always form there seasonally, as illustrated by Figure 2. They form during fall-winter, when the equatorial deposits and the CH_4 frosts at the opposite pole (spring-summer) feed the atmosphere with gaseous CH_4. In BF2016, a similar result was obtained but because the simulations were not performed with a large enough reservoir of CH_4 ice, no thick deposit was obtained at the equator and the polar frosts disapeared in the early spring.

3.3   Sensitivity to the reservoir, soil thermal inertia and CH_4 ice albedo

Changing the initial spatial distribution of CH_4 ice (e.g. only at the poles, or over a specific longitudinal or latitudinal band) does not impact the results: CH_4 ice would still accumulate at the equator, with a slight extent to northern latitudes, while mm-thin deposits would form elsewhere during polar winter. If we increase the CH_4 reservoir, then thicker CH_4 deposits are obtained at the equator. The CH_4 mid-to-polar frosts remain qualitatively and quantitatively the same year after year because they are controlled by the location of the equatorial deposits.

Changing the albedo of CH_4 ice leads to major changes in the results. If we lower the uniform CH_4 ice albedo, the ice becomes warmer, resulting in higher sublimation rates and larger amounts of CH_4 to be transported to other sinks. In this case, we obtain more extended equatorial deposits and episodic thicker perennial deposits at the poles (see middle panel on Figure 3). If we increase the uniform CH_4 ice albedo, then CH_4 ice may become cold enough to trigger N_2 condensation on it, which strongly impacts both volatile cycles. This effect is explored in Section 4.
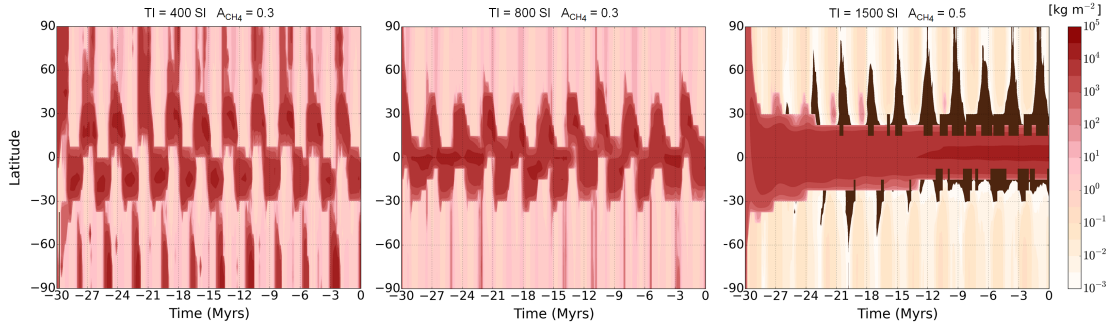
Fig. 3. Same as Figure 2 but assuming a thermal inertia TI=400 SI coupled with a
CH$_4$ ice albedo A$_{CH_4}$=0.3 (left), TI=800 SI and A$_{CH_4}$=0.3 (middle), TI=1500 SI
and A$_{CH_4}$=0.5 (right). The low TI case was performed with a lower albedo for CH$_4$
ice (0.3) in order to limit the effect of N$_2$ condensation on CH$_4$ ice (this effect is
explored in Section 4). The brown color represents the dark, tholin-covered bedrock.

Results are also sensitive to the soil thermal inertia, as shown in Figure 3.
When a high thermal inertia is used (> 1500 SI), surface temperatures tend
to be much warmer at the poles than at the equator on average over several
Myrs (see B2018) and thus CH$_4$ ice accumulates closer to the equator, while
less frost forms at the poles. When a low thermal inertia is used (< 400 SI),
the surface temperatures reach higher values in summer and lower values in
winter and tend to be warmer at the equator than at the poles on average over
several Myrs. In this case, large perennial reservoirs can form periodically in
the mid-to-polar regions. However this case predicts, for present time, large
reservoirs of CH$_4$ ice in the south hemisphere only, which is not consistent
with the observations.

4 Simulations with darker CH$_4$ ice near the equator than at mid and high latitudes

CH$_4$ ice is known to play a complex role on Pluto's climate and volatile ices
cycles since it can cold trap N$_2$ ice if its albedo is high enough (Bertrand and
Forget, 2016; Earle et al., 2018a). In our model, the albedo of CH$_4$ ice is a key
sensitivity parameter and we usually represent it by one value only, constant
with time. However, on Pluto, the real value is not very well known and varies
with time and space, because of different processes involving metamorphism ef-
fects, haze-particle settling/contamination (which serves as a darkening agent)
and slight differences of composition (Buratti et al., 2017; Stern et al., 2015).
As an example, CH$_4$-rich ice is much brighter in the mid-to-polar than in the
BTD (Buratti et al., 2017).

In this section, we intend to explore this sensitivity and better represent the

cycle of CH_4 by considering two different albedos for CH_4 ice in the model, based on a criterion in latitude. In accordance with New Horizons observations, we assume that the mid-to-polar deposits are bright (albedo=0.65-0.8) and that the equatorial massive CH_4 ice deposits are dark (albedo=0.5-0.65). We also explore the impact of TI on the results (TI=400-1200 SI). The albedos of the volatile-free surface and of N_2 ice remain always fixed to 0.1 and 0.7 respectively.

The results of this section are summarized in Section 4.7 by Figure 15 and Table 2. Note that all results shown for the current Pluto year are the outcome of 30 Myrs simulations.

4.1 Initial state of the simulations

N_2 ice is placed in Sputnik Planitia only. We place an unlimited CH_4 ice reservoir in the equatorial regions roughly at the locations of the observed BTD: 15°S-15°N, 140°W-15°E. The rest of the surface is initially volatile-free (assumed to be a tholin-covered water ice bedrock with an albedo of 0.1). We then run the simulations and let the volatile ices evolve over 30 Myrs.

4.2 Reference simulation: accumulation of CH_4 ice at mid-latitudes

Our reference simulation is named #TI888_050_072, which means that is the simulation performed with a thermal inertia (TI) of 800 SI for N_2, CH_4 and water ices, an albedo for CH_4 equatorial deposits of 0.5 and an albedo for CH_4 mid-to-polar deposits of 0.72.

4.2.1 The astronomical cycles of CH_4

Figure 4 shows the evolution of the perennial CH_4 (in red) and N_2 (blue markers) ice deposits obtained over the last 12 Myrs. In this reference simulation, mid-to-polar CH_4 deposits form at higher latitudes than 30°. Below, the equatorial regions remain volatile-free or covered by the modeled BTD, which is consistent with the observation of dark equatorial regions on Pluto (e.g Cthulhu). These CH_4 deposits are cold enough to trigger N_2 condensation and allow the formation of perennial or seasonal N_2 deposits. Those located around 30°N or 30°S remain perennial at all times, while those located at higher latitudes remain perennial only during 1-2 Myrs during each astronomical cycle, as shown in Figure 4. Note that these perennial N_2 ice deposits remain less than 15 m thick, as shown in Table 2. At the North Pole, thin perennial CH_4

17

deposits (< 1 m) alternate with seasonal deposits over an astronomical cycle. Between 60°N-75°N, perennial CH_4 ice deposits (< 1 m) remain stable with time, while at northern mid-latitudes (25°N-60°N), a net accumulation of CH_4 ice is obtained (Figure 4.B). The stability and accumulation of CH_4 ice at these latitudes is due to (1) the condensation of N_2 ice on top of the bright CH_4 ice, which is able to protect CH_4 from sublimation during most of the year and cold-trap even more CH_4, (2) the presence of infinite amounts of CH_4 ice at the equator (BTD), which continuously feed the atmosphere with gaseous CH_4. Indeed, the BTD are found to be a net sublimation zone of CH_4 ice over astronomical timescales, transporting CH_4 ice to the mid-to-polar regions. As shown in Table 2 and Figure 4, ~ 90 m of CH_4 ice are lost by the BTD and 30 m of CH_4 ice accumulated between 30°N-60° after 30 Myrs.

We performed the same simulations but starting at t_0 =-100, -200 and -300 Myrs, in order to verify if the transport of CH_4 ice from the BTD to the mid-latitudes also occurs in different configuration for Pluto's orbit (the entire period of the cycle obliquity + solar longitude of perihelion at maximum obliquity is 375 Myrs, as shown in Figure 5 in B2018). We obtained similar results. Consequently, assuming that the Milankovitch cycles on Pluto remain stable with time, if we let this simulation evolve over 1 billion years, 3 km of CH_4 ice would have been transferred from the BTD to the mid-latitudes, where CH_4 ice would form a 1 km thick mantle. These results are consistent with the observations of New Horizons showing that the mid-latitudes are covered by a kilometer-thick mantle of volatile ice (Howard et al., 2017). They suggest that CH_4 has been accumulated there since hundreds of Myrs by the action of N_2 condensation-sublimation, and that the BTD have been losing significant amounts of CH_4 ice by sublimation. We further discuss this point in Section 5.

4.2.2   The current seasonal cycle of CH_4

Figure 4 shows that, at astronomical scale, present-time Pluto is in a period of its Milankovitch cycle where N_2 and CH_4 perennial deposits are not favored at high latitudes, compared to other periods (such as 2 Myrs ago for instance). Figure 5 shows the latitudinal distribution of N_2 (in blue, mixed with CH_4) and CH_4 (in red, no N_2) ice obtained over a current Pluto year and after 30 Myrs of simulation.

In the northern hemisphere, we can distinguish three different regions in latitudes.

(1) Around the North Pole (above 75°N), CH_4 condenses as a thin frost (< 1 mm) during fall and triggers the condensation of N_2 ice on it during winter. When spring begins (Earth year 1988), the thin N_2 deposit
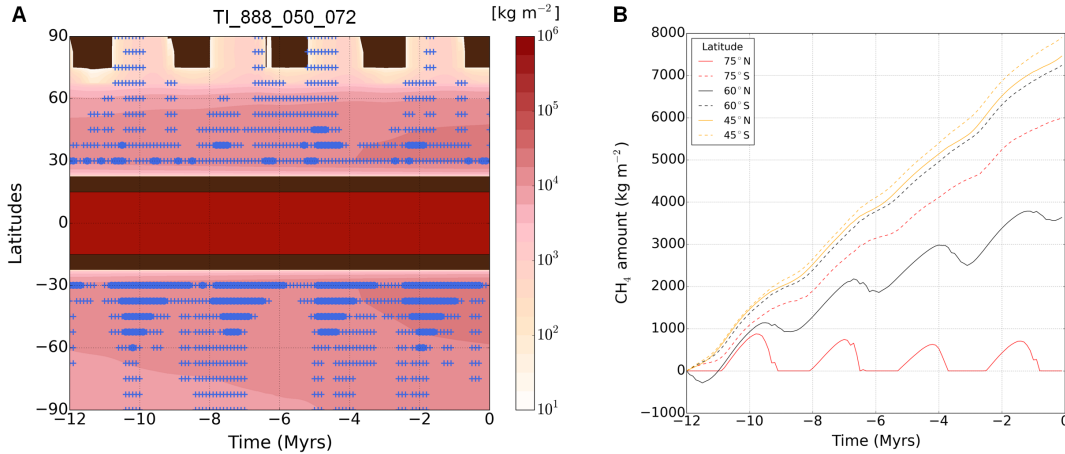
Fig. 4. Simulation #TI888_050_072. A. Evolution of the perennial CH_4 ice deposits: minimum amount of surface CH_4 ice (per Pluto year, over the last 12 millions of Earth years, that is ∼4 obliquity cycles). Seasonal deposits (frosts) are not shown. The dark-red band at the equator indicates the latitudes of the modeled BTD, which are an infinite source of CH_4 in the simulations. The dark-brown color represents the dark, tholin-covered bedrock. The blue markers (cross and star) indicate the presence of N_2 ice perennial deposits, which are obtained at low elevations only (patchy deposits: cross) or over all longitudes (latitudinal band: star). B. Variation of the amount of surface CH_4 ice as shown in the panel A, for different latitudes and normalized at t=-12 Myrs. At the northern polar latitudes, perennial deposits form and disappear at each astronomical cycle.

(< 1 cm) starts to sublime. It disappears around year 2000, revealing a bright thin CH_4 frost that will last until 2017 before disappearing and leaving the dark substrate volatile-free during the entire summer. This is consistent with Figure 4.A, which predicts that there is no perennial deposit at the North Pole for the current epoch.

(2) At mid-latitudes (45°N-75°N), seasonal 1-m thick N_2 ice deposits cover CH_4 ice during most of the year, except during late spring and summer. During this period, N_2 ice sublimes from the pole and reveals the CH_4 ice mantle which starts to sublime as well. However, over the entire Pluto year, there is a net accumulation of CH_4 ice at these latitudes, leading to the formation of a thick mantle of CH_4 ice over Myrs, as shown in Figure 4.A.

(3) Between 30°N-45°N, a perennial latitudinal band of N_2 ice is obtained.

The southern hemisphere is covered by up to 1 m thick N_2 ice deposits during most of the year except during late summer, where it sublimes from the pole and reveals the CH_4 ice mantle. Around 1988, when southern fall begins, N_2 ice condenses and first covers the South Pole and then the mid-latitudes. A net accumulation of CH_4 ice occurs in the southern hemisphere over seasonal and astronomical timescales.
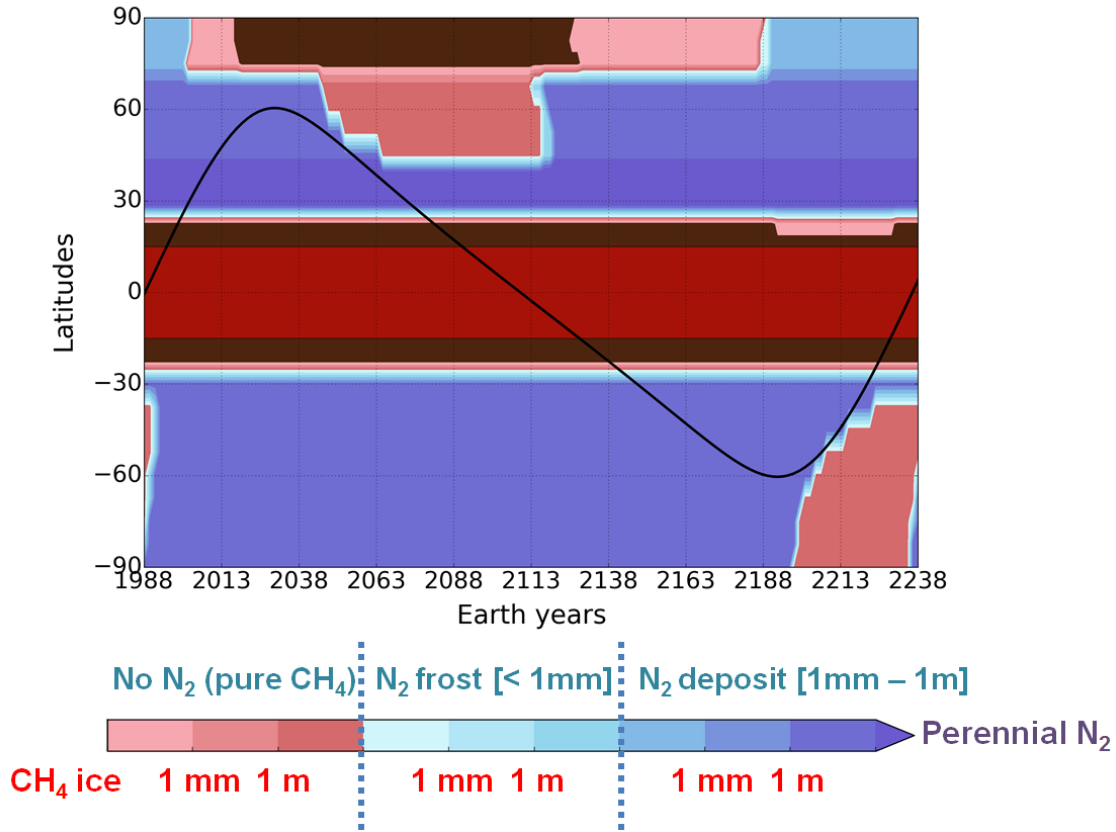
19

Fig. 5. Reference simulation #TI888_050_072. Evolution of the latitudinal distribution of the deposits over a current annual timescale (at longitude 0°). The solid dark line shows the position of the subsolar point with time. Blue colors indicate the presence of N_2 ice and CH_4 ice while red colors indicate the presence of CH_4 ice only. The lighter the color, the thinner is the deposit. The dark-red band at the equator indicates the latitudes of the modeled BTD, which are an infinite source of CH_4 in the simulations. The dark-brown color represents the dark, tholin-covered bedrock.

4.3 Sensitivity to the albedo of the equatorial CH_4 deposits

Three different scenarios are obtained in our simulations if we increase or decrease the albedo of the modeled BTD (A_{CH_4eq}):

(1) If $A_{CH_4eq} \ll 0.6$, the BTD are dark and warm enough so that they never trigger N_2 condensation. Lower albedo values lead to enhanced sublimation rates of CH_4 above these deposits and larger amounts of CH_4 ice transported to the mid-to-polar regions. For instance, Figure 6 shows the results obtained from simulation #TI888_030_072, performed with an equatorial CH_4 albedo of 0.3. In this simulation, up to 1 km of CH_4

20

ice has been lost from the BTD after 30 Myrs (Table 2), and transported to the mid-to-polar regions. In this case, CH_4 is able to remain around the north pole and form perennial deposits at all times.

(2) If $A_{CH_4eq} \approx 0.6$, condensation of N_2 occurs on the CH_4 equatorial deposits but only at low elevations (simulations #TI888_060_072, #TI888_060_080, #TI888_065_072, #TI888_065_080). The case of #TI888_065_072 is shown in Figure 7. Up to 200-300 m thick N_2 ice deposits form in the low-elevated equatorial regions where CH_4 ice is present (see blue-star markers on Figure 7.A and Max_{eqN_2} in Table 2). The high altitude BTD remain N_2-free and feed the atmosphere with gaseous CH_4 as they sublime, allowing the formation of perennial and seasonal CH_4 deposits at the poles. These mid-to-polar deposits are thinner than in the reference case because part of the equatorial source of gaseous CH_4 is trapped by N_2 ice.

(3) If $A_{CH_4eq} \gg 0.6$, then the BTD are bright enough to trigger N_2 condensation at most altitudes. They are covered and cold trapped by 200-300 m of N_2 ice (see Table 2), mostly in the low-elevated regions since this is enough N_2 to flow downhill. These N_2 deposits remain relatively stable at such equatorial latitudes, as demonstrated by B2018 as well. In this case, the CH_4 sublimation at the equator is limited and thus there is not enough gaseous CH_4 available to form mid-to-polar deposits. As a result, Pluto's surface outside the equatorial regions remains volatile-free, which is not realistic (no simulation result is shown for this case).

To summarize, Table 2 shows that the amount of CH_4 ice lost by the modeled BTD over 30 Myrs is about 1 m, 10 m, 100 m or 1000 m assuming a CH_4 ice albedo of 0.65, 0.6, 0.5, or 0.3 respectively.
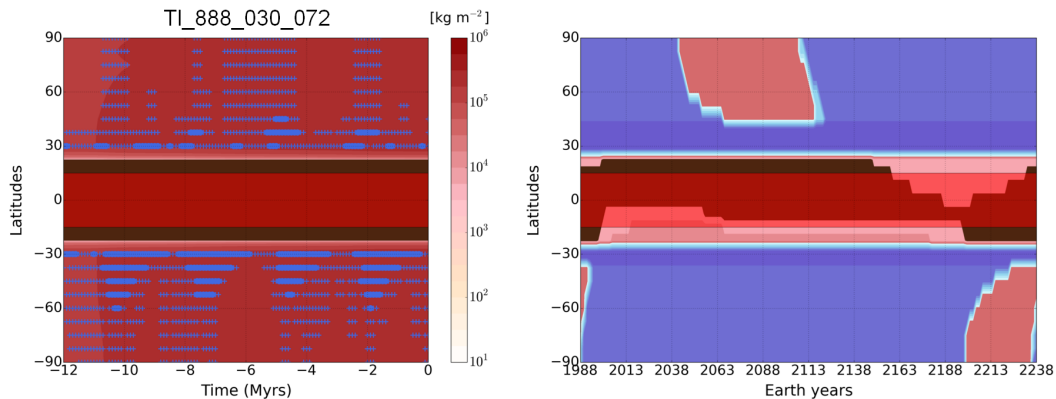

Fig. 6. Simulation #TI888_030_072. Same as Figure 4 and Figure 5 (legends are the same), except for an equatorial CH_4 ice albedo of 0.3 (very dark BTD).
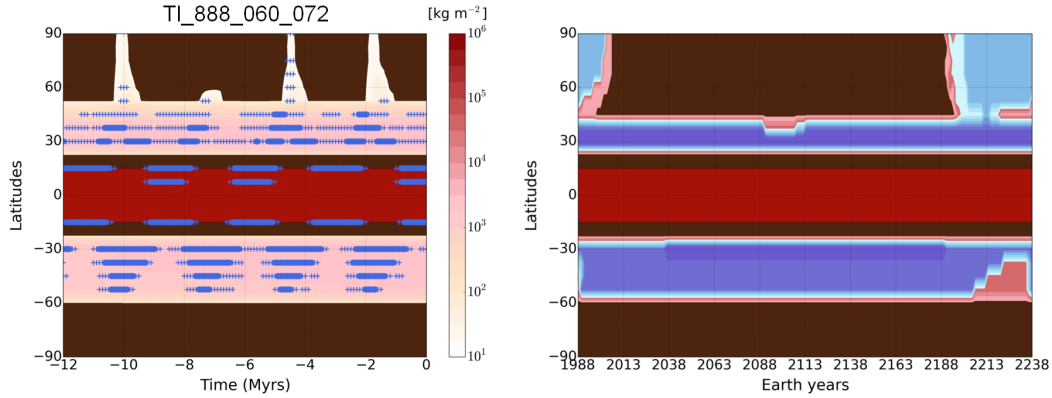
21

Fig. 7. Simulation #TI888_060_072. Same as Figure 4 and Figure 5, except for an equatorial CH$_4$ ice albedo of 0.60 (relatively bright BTD).

4.4 Sensitivity to the albedo of the mid-to-polar CH$_4$ deposits

Our results are also very sensitive to the albedo of the mid-to-polar CH$_4$ ice deposits. When this albedo is higher than 0.6, N$_2$ ice tends to condense on the CH$_4$ ice during fall-winter and form seasonal (few mm thick) or perennial deposits (up to 20 m thick), as shown for the reference case by Figure 4 and Figure 5. If the mid-to-polar CH$_4$ ice albedo is lower than 0.6, then only thin seasonal frosts of CH$_4$ are obtained at the poles during fall-winter, as they do not trigger N$_2$ condensation. This case corresponds to the results obtained in Section 3 and in BF2016.

The higher the albedo of mid-to-polar CH$_4$ ice, the more N$_2$ condenses, at higher latitudes, and the longer it remains and traps CH$_4$ during Pluto's year. For instance, in our simulation using a mid-to-polar CH$_4$ ice albedo of 0.65 (#TI888_050_065, Figure 8), we obtain perennial N$_2$ deposits at 30°N and very thin seasonal N$_2$ deposits at higher latitudes and in the southern hemisphere above 50°S. As a result, CH$_4$ ice does not form thick deposits outside 50°N-50°S, but only seasonal frosts (e.g. the northern polar frost quickly disappears after 2013).

This is to be compared with the reference simulation (Figure 4 and Figure 5), where the brighter mid-to-polar CH$_4$ ice albedo (0.72) triggers N$_2$ condensation at higher latitudes and leads to thick CH$_4$ ice deposits up to 70°N and 90°S, while the northern polar frost quickly disappears after 2017.

Finally, in the more extreme case of a mid-to-polar ice albedo of 0.8 (#TI888_050_080, Figure 9), perennial deposits of N$_2$ ice extend up to the pole during half of an

22

obliquity cycle. During the current-year Pluto, N_2 ice covers the bright CH_4 ice up to the poles during most of the year, except during a short period in summer. In this simulation, long term accumulation of CH_4 ice is obtained everywhere outside the equatorial regions.
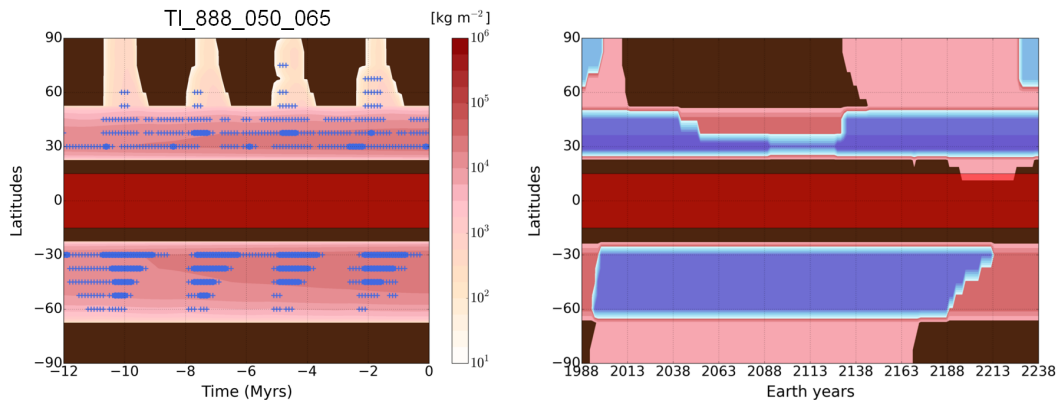

Fig. 8. Simulation #TI888_050_065. Same as Figure 4 and Figure 5, except for a mid-to-polar CH_4 ice albedo of 0.65.
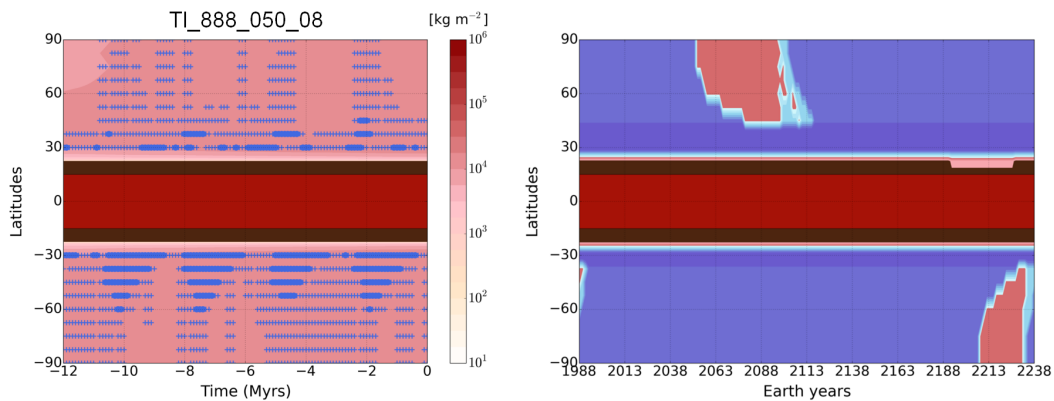
Fig. 9. Simulation #TI888_050_080. Same as Figure 4 and Figure 5, except for a mid-to-polar CH_4 ice albedo of 0.8.

4.5 Sensitivity to N_2 ice phase emissivity

The emissivity of N_2 ice in its α-phase is less than that in its β-phase (Stansberry and Yelle, 1999; Lellouch et al., 2011b). Here we tested the sensitivity of the results to the N_2 ice emissivity by assuming that it varies between ε_α=0.3 in α-phase and ε_β=0.8 in β-phase, as described in Section 2.3. This assumption

has a strong impact on the N_2 cycle because the change of emissivity forces the ice surface temperature to remain at the transition temperature $T_{\alpha-\beta}$=35.6 K during most of Pluto's northern fall and winter. Consequently, higher annual mean N_2 ice surface temperature and surface pressure are obtained.

Figure 10 shows the results obtained for simulation #TI888_050_072_phase, which reproduces the reference simulation but taking into account the change of N_2 ice emissivity. The main differences with the results from the reference simulation (Figure 4 and Figure 5) are: (1) N_2 ice does not form thick perennial deposits outside Sputnik Planitia. Over a current annual timescale, N_2 ice deposits in the mid-to-polar regions are only seasonal and disappear during summer. In the last 12 Myrs, perennial deposits are obtained only at low elevations, (2) No N_2 ice forms at the south pole during a current Pluto year, (3) CH_4 ice does not accumulate above 50°N and below 70°S.

Consequently, the decrease of N_2 ice emissivity with temperature is an example of negative feedback which would limit the formation of N_2 deposits outside Sputnik Planitia.
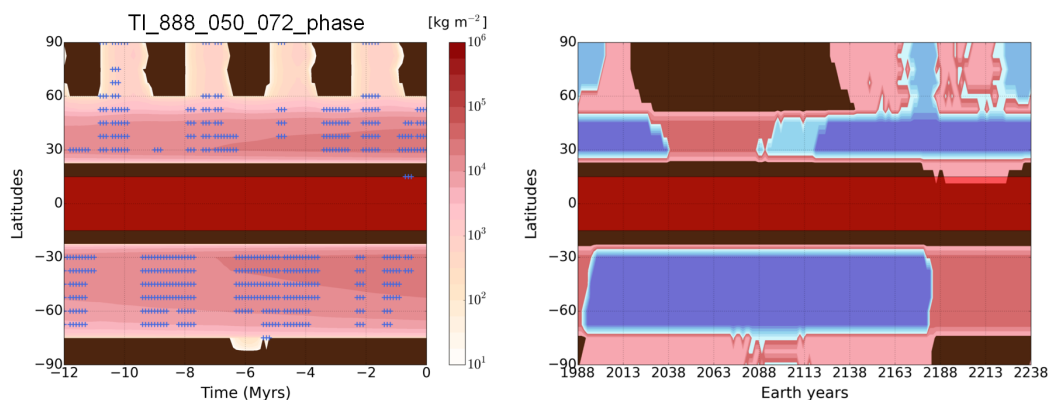
Fig. 10. Simulation #TI888_050_072_phase. Same as Figure 4 and Figure 5, except that the N_2 ice emissivity varies according to its phase (α or β) from ε_α=0.3 to ε_β=0.8.

4.6 Sensitivity to the thermal inertia of the different ices

In the previous sections, simulations have been performed assuming a global uniform thermal inertia. In reality, the ices have different thermal inertia as it depends on the porosity of the material, the size of grains (larger grains lead to higher thermal inertia)... In this section, we allow each ice to have its own TI in the model, ranging from 400 SI to 1200 SI, and we explore the impact

of these changes on the results (summarized in the second part of Table 2).

For instance, simulation #TI8412_050_065 has been performed with a thermal inertia of 800 SI for N_2 ice (8), 400 SI for CH_4 ice (4) and 1200 SI (12) for the water ice bedrock. In the model, TI evolves with time depending on the new thickness of the volatile ice on Pluto's surface. If a 1 m thick layer of CH_4 ice lies on water ice in the model, then the TI is set to 400 SI over the first meter of the subsurface and to 1200 SI below (in practice in the model the conductivity is modified to correspond to the required thermal inertia).

Changing the TI of N_2 ice (e.g. simulations #TI488 or #TI1288) does not significantly change the ice distribution. This is because to first order, the variation of the exchanged mass of N_2 between the surface and the atmosphere is independent of thermal inertia, as detailed in Section 2.2 in B2018.

Changing the TI of CH_4 ice has also little impact on the ices distribution. Lower values of TI allows for colder CH_4 ice during winter, and eventually to slightly larger seasonal and perennial reservoirs of N_2 ice at the poles (simulations #TI848,#TI8412). The impact is also limited by the fact that the simulated CH_4 ice deposits are thin (few meter thick), because the initial reservoir is low (see Section 2.4).

Changing the TI of water ice has a significant impact on the thin volatile ice deposits, and therefore mostly at the poles. Low TI allows colder poles in winter and the formation of thicker CH_4 and N_2 deposits there (simulations #TI884). For instance, in the case of a mid-to-polar CH_4 ice albedo of 0.65 (#TI884_05_065, Figure 11), the northern polar N_2 deposit remains until years 2015-2020, and the CH_4 frost until 2025. This is to be compared with simulation #TI888_05_065 (Figure 8), where the northern frosts only last until 2000 and 2010 respectively, and where no N_2 condenses at the south pole. The effect is even stronger if we compare #TI884_05_072 (Figure 13) with the reference case TI888_05_072 (Figure 5). The N_2 polar deposit remains longer in northern spring and disappears after 2038, while the polar frost of CH_4 remains during the entire Pluto year.

To summarize, our results are much less sensitive to TI (in the range 400-1200 SI) than albedos, although the TI of the water ice bedrock significantly impacts the distribution of the thin polar deposits.

4.7   Summary of simulation results

Figure 15 gives an overview of the different simulations performed in this Section 4 and the different ices distributions obtained depending on the assumed albedo for CH_4 ice. Figure 15.1 shows how the simulations were initialized:
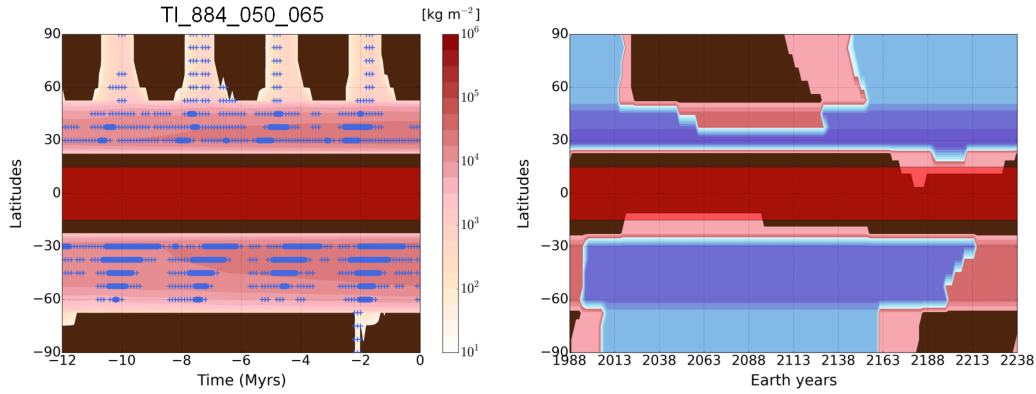
Fig. 11. Simulation #TI884_050_065. Same as Figure 4 and Figure 5, except for a mid-to-polar CH_4 ice albedo of 0.65 and a TI for water ice of 400 SI.
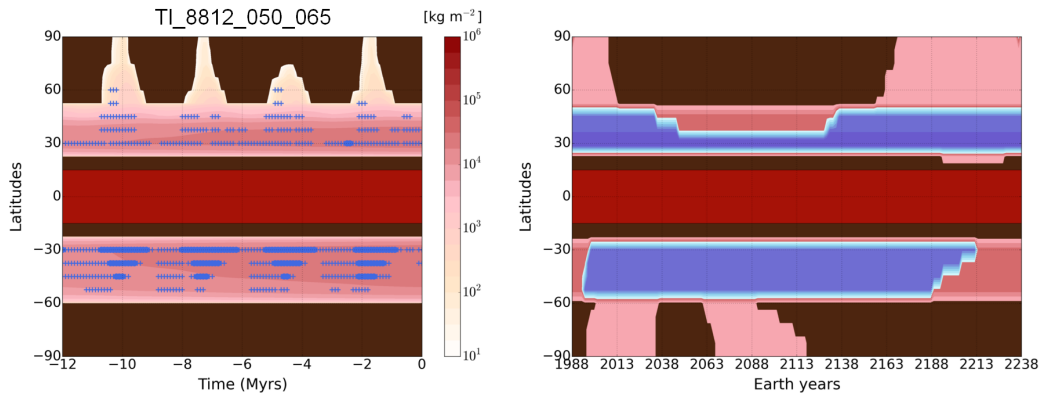

Fig. 12. Simulation #TI8812_050_065. Same as Figure 4 and Figure 5, except for a mid-to-polar CH_4 ice albedo of 0.65 and a TI for water ice of 1200 SI.

N_2 ice fills Sputnik Planitia while unlimited amounts of CH_4 ice are placed roughly at the location of the BTD. If the CH_4 ice albedo remains well below 0.6, only seasonal CH_4 frosts form at the poles, as shown in Figure 15.2. If the modeled BTD have an albedo well above 0.6 (Figure 15.3), then they become cold enough to trigger N_2 condensation. The N_2 ice deposits thus formed trap the CH_4 ice, which cannot feed the atmosphere with gaseous CH_4. As a result, there is no gaseous CH_4 left in the system and no frost can form at the poles, which remain volatile-free at all times. Using an albedo for the BTD around 0.6 allows the formation of N_2 ice deposits only in the depressions of these terrains, as shown in Figure 15.4. The high-altitude BTD remains N_2-free and feed the system with CH_4, allowing the formation of seasonal frosts at the
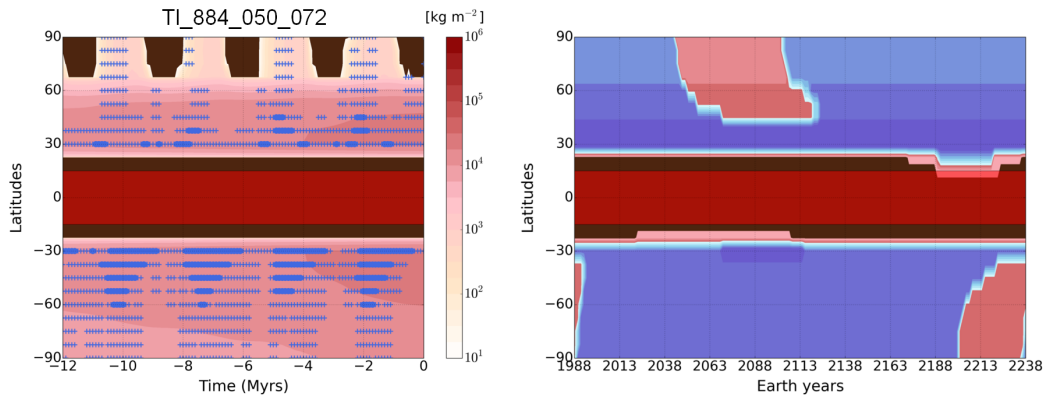
Fig. 13. Simulation #TI884_050_072. Same as Figure 4 and Figure 5, except for a TI for water ice of 400 SI.
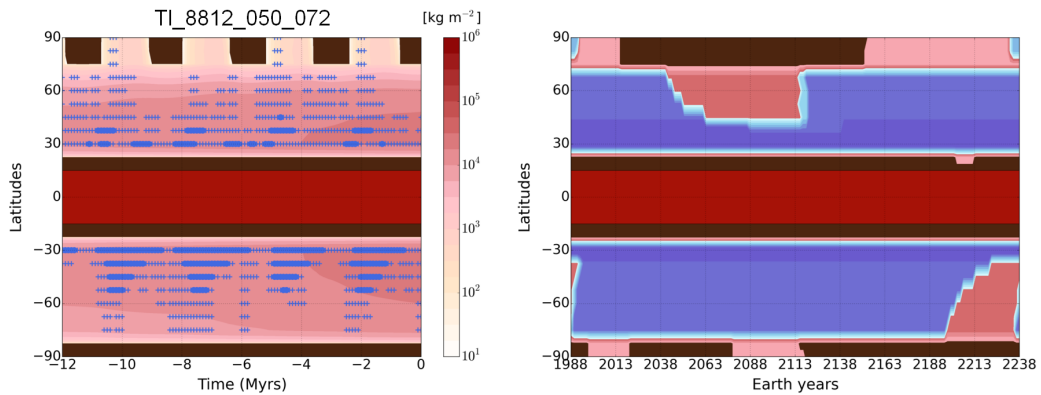
Fig. 14. Simulation #TI8812_050_072. Same as Figure 4 and Figure 5, except for a TI for water ice of 1200 SI.

poles. Finally, if the albedo of the mid-to-polar CH_4 deposits is set higher than 0.6 (Figure 15.5), then N_2 can condense and form thin seasonal deposits at the poles and larger deposits at mid-latitudes, which can be perennial or seasonal (up to few tens of meter thick, in particular in depressions). These N_2 deposits are able to trap large amounts of CH_4 ice, resulting in the formation of a thick mid-latitudinal mantle of CH_4 ice.

1. Initial ices distribution

Final states in the cases of :
2. Equatorial and polar CH_4 albedo << 0.6
3. Equatorial CH_4 albedo >> 0.6
4. Equatorial CH_4 albedo ≈ 0.6, Polar << 0.6
5. Equatorial CH_4 albedo ≈ 0.6, Polar >> 0.6

1 Spuntik Planitia

Bladed Terrain deposits

Volatile-free surface (dark)	Dark CH_4 deposits	Bright CH_4 deposits	N_2 deposits

(S) Seasonal deposits (P) Perennial deposits (SP) Seasonal or perennial deposits

Fig. 15. Summary of the simulation obtained in Section 4.

4.8 Surface pressure and CH_4 atmospheric mixing ratio

4.8.1 The peak surface pressure during northern spring

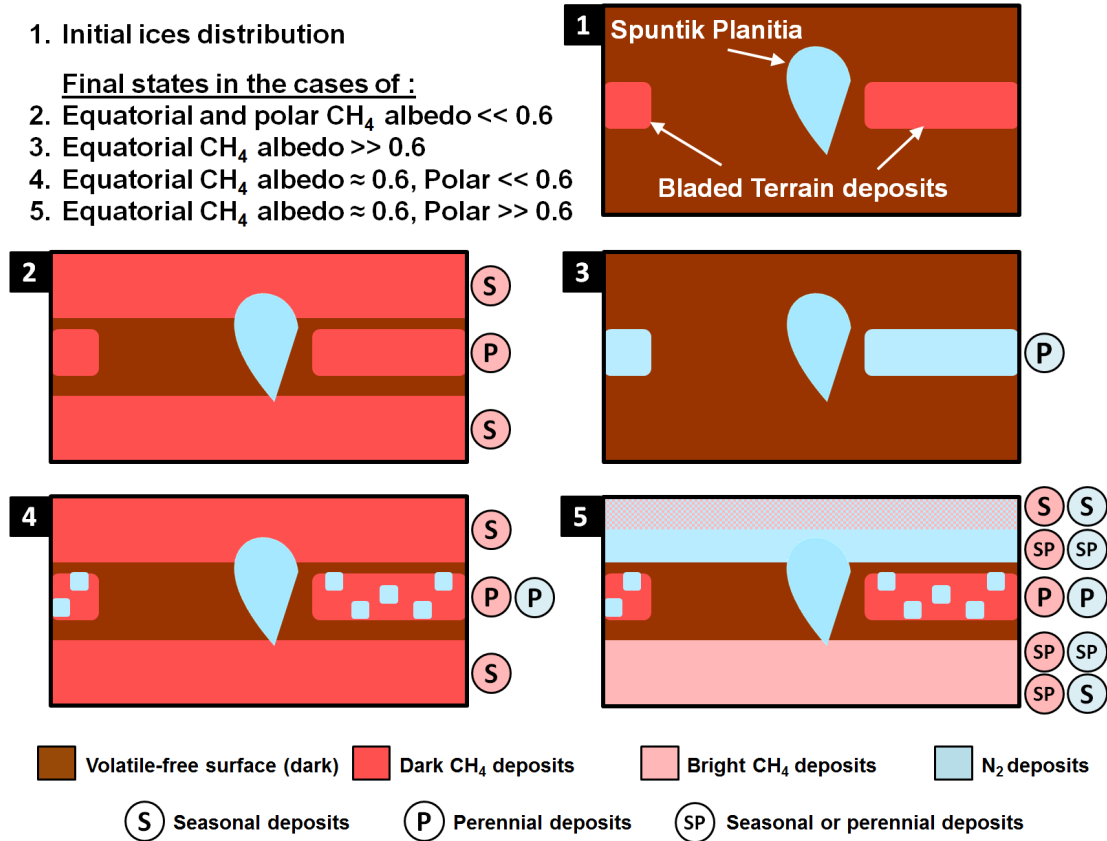Simulations from BF2016 predicted an evolution of surface pressure in accordance with the stellar occultation observations conducted from Earth since 1988. The threefold increase of pressure observed would result from N_2 ice heating when (1) Sputnik Planitia is most exposed to sunlight (shortly after the northern spring equinox in 1989) and (2) Pluto is close to the Sun. Their model also predicts that the atmospheric pressure should decrease in the following decades, after reaching its maximum around 2015, because of the orbitally-driven decline of insolation above Sputnik Planitia.

Here, in this paper, although the general aspect of the annual evolution of surface pressure remains unchanged (see Figure 2.a in BF2016), the peak surface pressure occurs earlier than 2015 in many of our simulations. The main differences between the simulations of this paper and those from BF2016 are the presence of N_2 ice deposits outside Sputnik Planitia that slightly affect the evolution of pressure (by enhancing the global condensation or sublimation

28

flow) and the better resolution of the Sputnik Planitia basin (BF2016 only assumed a circular crater).

Our simulations show that the annual pressure peak occurs when the area of the sublimation source in the northern hemisphere becomes less than the area of the condensation sink in the southern hemisphere. For instance, in the reference simulation (#TI888_050_072), the peak occurs in year 2000 when the northern polar deposit of N_2 disappears.

Simulations with a peak surface pressure occurring after 2010 are (1) the ones with a very high mid-to-polar CH_4 albedo, leading to both hemispheres covered by N_2 ice during northern spring (these cases are not realistic because they do not correspond to the ice distribution observed by New Horizons), (2) the ones with a thermal inertia for water ice around 400 SI (#TI444, #TI884, #TI12124). In these cases, the thin northern polar deposit of N_2 lasts until 2010-2015, (3) The ones without N_2 ice outside SP (like in BF2016). This scenario is only obtained when using in the model a dark mid-to-polar CH_4 albedo (less than 0.6).

These results suggest that the southern hemisphere of Pluto is not entirely covered by N_2-rich ice, otherwise the peak surface pressure would have occurred much earlier than 2015 (a similar result is found in Young (2013); Olkin et al. (2015)). At most, a thin mid-latitude band of N_2-rich ice (similar to that observed in the northern hemisphere) could be present in the southern hemisphere in 2015.

4.8.2   Evolution of surface pressure over astronomical timescales

In all simulations of this paper, the surface pressure obtained remains within few mPa-Pa, with a maximal value of 4 Pa over 30 Myrs. This is in the same range than the values obtained in B2018 (see Figure 16 of their paper, lines obtained with an albedo of 0.7 for N_2 ice). We could have expected higher values in the results of this paper because we obtained N_2 deposits at the poles. However, the increase of pressure due to their sublimation in summer is always balanced by the strong condensation flux at the opposite pole.

4.8.3   Evolution of CH_4 atmospheric mixing ratio over astronomical timescales

The atmospheric mixing ratio of CH_4 obtained is very sensitive to model parameters (Bertrand and Forget, 2016), in particular those controlling the BTD (main source of gaseous CH_4). Figure 16 shows the annual maximum and minimum values obtained over astronomical timescales for different simulations. We note that (1) The CH_4 atmospheric mixing ratio remains within 0.001-1% in most of the simulations, including the reference case, (2) Higher values

can be obtained for a lower equatorial CH_4 albedo (0.01-10% with an albedo of 0.3), (3) Lower values are obtained when N_2 condenses on the equatorial CH_4 deposits (10^{-4}-10^{-2}%), (4) The lower the albedo of the mid-to-polar CH_4 deposits, the higher the concentration of CH_4 in the atmosphere (because of the higher equilibrum temperature and pressure of CH_4 and because there is less N_2 deposit forming and therefore more CH_4 ice available to feed the atmosphere with gaseous CH_4).
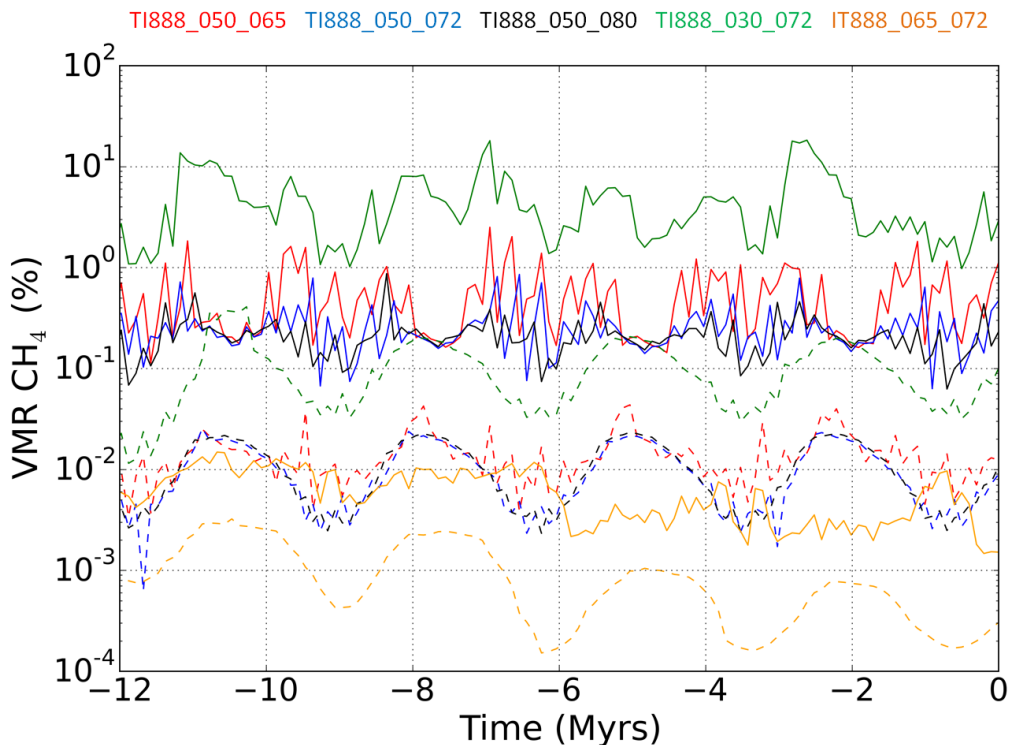
Fig. 16. Evolution of the annual maximum (solid line) and minimum (dashed line) global mean atmospheric mixing ratio of CH_4 for different simulations of this paper.

4.8.4   Opacity of Pluto's atmosphere at Lyman-α wavelengths

On Pluto, solar ultraviolet light is dominated by Lyman-α photons, which control much of the photodissociation of CH_4 and of the subsequent hydrocarbon photochemistry (Gladstone et al., 2016; Grundy et al., 2018). Bertrand and Forget (2017) showed that the photochemical reactions are photon-limited in present-day Pluto's atmosphere, i.e. that enough gaseous CH_4 is present for all photons to be absorbed by CH_4 molecules.

Here we want to assess the opacity of Pluto's atmosphere at Lyman-α wavelengths over astronomical timescales. Indeed, if the atmospheric mixing ratio of CH_4 or the entire atmosphere collapsed in Pluto's past, then a direct photolysis of surface ices and tholins could have happened, which would help

understanding the high degree of processing of the dark material in Cthulhu (Grundy et al., 2018).

To do that, we first estimate the total incident flux of Lyman-α at Pluto over one orbit (F_{tot}), considering the solar as well as the interplanetary medium (IPM) Lyman-α sources (Gladstone et al., 2015), as given by Eq. 2 and Eq. 5 in Bertrand and Forget (2017):

$$F_{tot}(d_p) = \frac{F_{Earth}}{4d_p^2} * 0.875 + F_{IPM} \tag{2}$$

We assume a constant solar Lyman-α flux at Earth F_{Earth}=4×10^{15} ph m^{-2} s^{-1}, a constant IPM flux at Pluto F_{IPM}=7.25×10^{11} ph m^{-2} s^{-1} and a constant extinction factor of 0.875. The IPM flux does not strongly depend on the Sun-Pluto distance d_p (Gladstone et al., 2015), therefore we consider it constant over time. The integration of F_{tot} over one Pluto orbit gives an annual mean incident Lyman-α flux of 1.3×10^{12} ph m^{-2} s^{-1}. We then use Eq. 1 in B2018 to estimate the fraction of this incident Lyman-α flux reaching the surface (Beers law), by feeding this equation with the values of surface pressure and atmospheric CH$_4$ mixing ratio obtained from our simulations over 30 Myrs.

Figure 17 shows the results for the same simulations than those shown on Figure 16. The atmosphere remains relatively opaque at Lyman-α wavelengths over astronomical timescales. For the most realistic simulations, the fraction of the annual mean incident flux that reaches the surface varies between 0.01 and 10% over time, with the lowest values obtained during high-obliquity periods, when mid-to-polar N$_2$ ice deposits are less stable. Over a current-year Pluto, we estimate that the fraction of Lyman-α reaching Pluto's surface is less than 1% of the total flux received. These fractions of Lyman-α flux may be sufficient to have a significant effect on the chemistry of the N$_2$:CH$_4$:CO ice mixtures (Materese et al., 2015; Grundy et al., 2018). Indeed, even if most of the Lyman-α flux is greatly attenuated most of the time, the photolysis of the ices goes on, albeit more slowly.

The fraction becomes negligible when the atmohere is enriched in gaseous CH$_4$, as it is the case if a low albedo of the equatorial CH$_4$ deposits is considered (#TI888_030_072, green line). However, most of the incident flux can reach the surface if the atmospheric CH$_4$ mixing ratio is less than 0.01% over an entire year, as it is the case for the simulations where N$_2$ covers the equatorial CH$_4$ deposits (#TI888_065_072, orange line). In this case, the CH$_4$ cycle is disrupted because the sources of gaseouse CH$_4$ are trapped by N$_2$ ice, and CH$_4$ can no longer block the energetic radiation, which would act directly on Pluto's surface ices.

Table 2. Settings and results of the simulations performed from 30 Myrs ago to present-day. From left to right, settings are: Run name (* indicates that the run is illustrated by figures in this paper), thermal inertia of N_2, CH_4, H_2O ice, equatorial and mid-to-polar CH_4 albedo. Results are: Loss of equatorial CH_4 ice after 30 Myrs, year of maximum pressure in current epoch, latitudes between which perennial N_2 ice deposits (pN_2) are obtained in the northern hemisphere, maximal thickness of these perennial deposits, same for seasonal deposits (sN_2), and maximal thickness of the equatorial N_2 ice deposits (formed on the modeled BTD).

| Name	TI_{N_2}	TI_{CH_4}	TI_{H_2O}	A_{CH_4} eq	A_{CH_4} poles	L_{CH_4}	Y_p	Lat_{pN_2}	Max_{pN_2}	Lat_{sN_2}	Max_{sN_2}	Max_{eqN_2}
			$(\mathrm{J\ s^{-1/2}\ m^{-2}\ K^{-1}})$			(m)		(°)	(m)	(°)	(m)	(m)
#TI888_050_060	800	800	800	0.5	0.6	75	1998.6			30-90	0.33	0
#TI888_050_065*	800	800	800	0.5	0.65	87	1996.9	30	1.5	37.5-90	0.51	0
#TI888_050_068	800	800	800	0.5	0.68	88	1995.1	30	4.0	37.5-90	0.59	0
#TI888_050_072*	800	800	800	0.5	0.72	91	2000.4	30-37.5	4.9	45-90	0.75	0
#TI888_050_080*	800	800	800	0.5	0.8	92	2017.9	30-37.5	7.3	45-90	0.90	0
#TI888_050_065_phase	800	800	800	0.5	0.65	72	2000.4			30-90	0.08	0
#TI888_050_072_phase*	800	800	800	0.5	0.72	86	1998.6			30-90	0.34	0
#TI888_050_080_phase	800	800	800	0.5	0.8	88	2017.9			30-90	0.77	0
#TI888_030_065	800	800	800	0.3	0.65	1794	1996.9	30-37.5	3.2	45-90	0.54	0
#TI888_030_072*	800	800	800	0.3	0.72	1776	2014.4	30-37.5	8.6	45-90	0.76	0
#TI888_060_072*	800	800	800	0.6	0.72	10	1996.9	30	4.9	37.5-90	0.66	77
#TI888_060_080	800	800	800	0.6	0.8	6	2000.4	30-37.5	7.7	45-90	0.86	97
#TI888_065_072	800	800	800	0.65	0.72	3	2002.1			52.5-90	0.11	357
#TI888_065_080	800	800	800	0.65	0.8	1	1996.9	30-37.5	4.7	45-90	0.68	185
#TI884_050_065*	800	800	400	0.5	0.65	85	2014.4	30	10.5	22.5-90	0.51	0
#TI884_050_072*	800	800	400	0.5	0.72	90	2019.6	30-37.5	6.2	22.5-90	0.81	0
#TI8812_050_065*	800	800	1200	0.5	0.65	85	1995.1	30	3.8	37.5-90	0.44	0
#TI8812_050_072*	800	800	1200	0.5	0.72	91	2014.4	30-37.5	14.6	45-90	0.70	78
#TI848_050_065	800	400	800	0.5	0.65	106	1996.9	30	5.5	45-90	0.58	72
#TI848_050_072	800	400	800	0.5	0.72	106	2005.6	30-37.5	9.4	37.5-90	0.78	0
#TI8128_050_065	800	1200	800	0.5	0.65	67	1996.9	30	2.0	37.5-90	0.47	0
#TI8128_050_072	800	1200	1200	0.5	0.72	73	1998.6	30	11.2	37.5-90	0.71	0
#TI1488_050_065	400	800	800	0.5	0.65	86	1995.1	30	2.4	45-90	0.51	0
#TI1488_050_072	400	800	800	0.5	0.72	90	2002.1	30-37.5	5.5	37.5-90	0.77	0
#TI11288_050_065	1200	800	800	0.5	0.65	87	1995.1	30-37.5	2.8	45-90	0.57	0
#TI11288_050_072	1200	800	800	0.5	0.72	92	2000.4	30-37.5	6.2	22.5-90	0.74	0
#TI1444_050_072	400	400	400	0.5	0.72	105	2010.9	30	8.3	22.5-90	0.77	91
#TI1444_050_080	400	400	400	0.5	0.8	105	2016.1	30	6.7	22.5-90	0.93	105
#TI844_050_060	800	400	400	0.5	0.6	100	2010.9	30	7.3	22.5-90	0.46	22
#TI844_050_065	800	400	400	0.5	0.65	108	2014.4	30-37.5	10.9	22.5-90	0.56	82
#TI844_050_072	800	400	400	0.5	0.72	108	2014.4	30-37.5	10.2	37.5-90	0.79	83
#TI8412_050_065	800	400	1200	0.5	0.65	133	1996.9	30	6.3	45-90	0.56	72
#TI8412_050_072	800	400	1200	0.5	0.72	108	1995.1	30-37.5	15.5	37.5-90	0.73	82
#TI8124_050_060	800	1200	400	0.5	0.6	59	2007.4			30-90	0.31	0
#TI8124_050_065	800	1200	400	0.5	0.65	66	2012.6	30-37.5	5.0	22.5-90	0.49	0
#TI8124_050_072	800	1200	400	0.5	0.72	72	2019.6	30-37.5	6.4	22.5-90	0.81	0
#TI81212_050_065	800	1200	1200	0.5	0.65	66	1995.1	30	2.1	37.5-90	0.50	0
#TI81212_050_072	800	1200	1200	0.5	0.72	71	1996.9	30	6.1	37.5-90	0.63	0
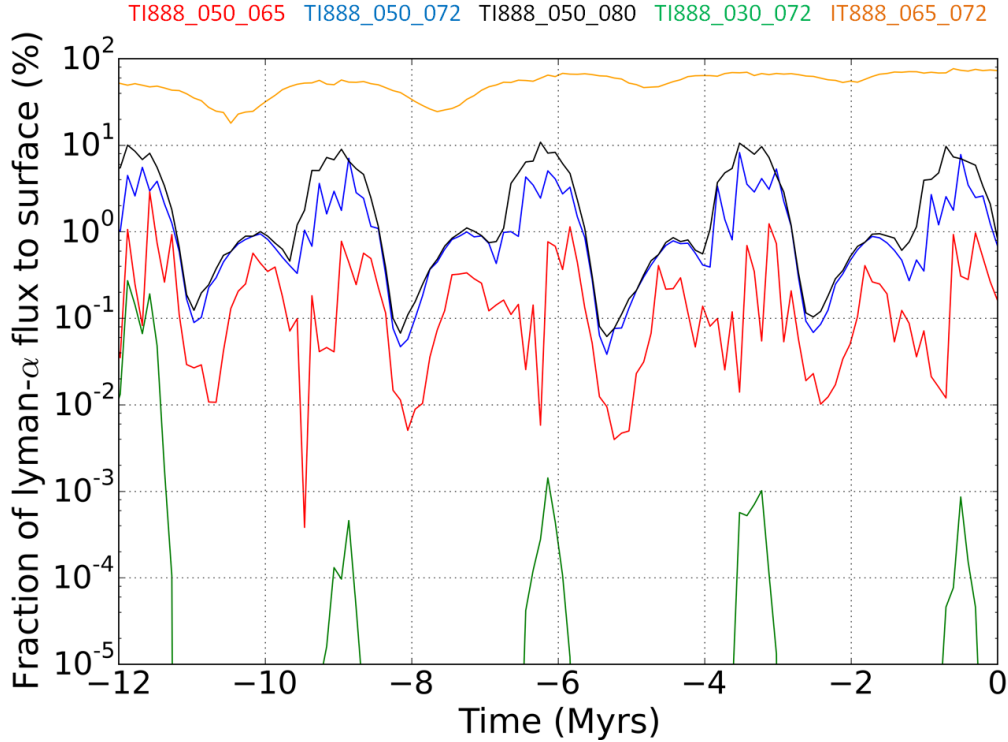
Fig. 17. Fraction of Lyman-α flux reaching Pluto's surface (on annual average) for the same simulations than on Figure 16.

5 Discussions

In this section, we first compare our results with Pluto's observations and further discuss the possible scenarios for the formation and evolution of the N_2 and CH_4 reservoirs.

5.1 Comparison of our results with Pluto's observations

5.1.1 The massive equatorial CH_4 deposits

In our model, CH_4 ice spontaneously tends to accumulate in the equatorial regions over astronomical timescales (see Section 3), forming thick perennial CH_4 deposits. This explains the presence of the massive equatorial CH_4-rich Bladed Terrain Deposits observed by New Horizons (Moore et al., 2016, 2018; Earle et al., 2018b).

We obtain a slightly larger accumulation of CH_4 ice north of the equator, which is consistent with the observed extension of the BTD, ranging in latitude from about 5°S to 28°N (see Fig. 4 in Earle et al., 2018b; Moore et al., 2018). This

location is reproduced by our simulations when assuming a medium-to-high soil thermal inertia (Figure 2). Similar results are obtained by starting the same simulation at another epoch. The equatorial deposits are also slightly more extended to the north if we start the simulation at t_0 =-100 Myrs, but to the south if we start at t_0 =-200 or -300 Myrs, which are assumed to be different epochs with a perihelion occurring at northern fall or winter during maximum obliquity periods (Figure 5 in B2018).

Our results show that 30 Myrs is too short a period of time to form km-thick equatorial CH_4-rich deposits like the BTD. The BTD may be relatively old, as suggested by their dark albedo ($\sim$ 0.5, Buratti et al. (2017)). The lack of craters suggests an upper limit on their age of 300 Myrs (Moore et al., 2018), although ancient craters may have been erased by intense sublimation of these terrains. We estimate that $\sim$ 1 km thick CH_4-rich deposits could form in the equatorial regions (30°S-30°N) over 50-100 Myrs, assuming an initial reservoir elsewhere (e.g. at the poles as in Section 3). Once this reservoir is depleted, extra hundreds of Myrs would be necessary to collect CH_4 ice from the edges of the equatorial regions toward more equatorial latitudes and to pile up km-thick amounts of ice. If the BTD are only few hundreds meter thick, they could have formed over 50 Myrs or less.

In the model, the equatorial CH_4 deposits form at all longitudes outside Sputnik Planitia. In reality, on Pluto, the unusual color of these terrains is only seen between longitudes 210°E to 40°E (Olkin et al., 2017; Moore et al., 2018; Earle et al., 2018b), and ground-based observations support the presence of more CH_4-rich deposits at these longitudes (Grundy and Buie, 2001; Grundy et al., 2013). This longitudinal asymmetry must be investigated with a full 3D Global Climate Model since it may be due to a dynamical effect of Pluto's atmosphere.

We also show in Section 4 that if the mid-to-polar CH_4 deposits are bright enough (we evaluate the critical CH_4 albedo around A_{CH4}=0.6), then mm-thick seasonal or meter-thick perennial N_2 deposits can form in these regions, preferentially at low elevations. In this case, we find that the BTD are not stable and correspond to a net sublimation zone at the astronomical timescale, because CH_4 ice is transferred from the BTD toward the mid-latitudes regions where it remains trapped by the perennial or seasonal N_2 deposits. Assuming a CH_4 albedo of 0.5 for the modeled BTD, we obtain a loss L_{CH_4} $\sim$100 m of ice over the 30 Myrs in most of our simulations (see Table 2). The km-thick BTD could therefore disappear within 300 Myrs.

These results suggest that the BTD were thicker in the past, and are now gradually disappearing. This is to be related to their bladed morphology, thought to be controlled by sublimation process (Moores et al., 2017; Moore et al., 2017, 2018).

5.1.2 The perennial reservoirs of N_2 ice

Our simulations show that, the closer to the equator, the more perennial are the N_2 reservoirs (outside of Sputnik Planitia). As a general trend, our model simulates two types of perennial N_2 reservoirs (apart from Sputnik Planitia). First, up to 200-300 m thick N_2 ice deposits can form at the equator, at low elevations where relatively bright CH_4 ice remains (albedo $\sim$0.6). This result is consistent with the detection of N_2 ice in East Tombaugh Regio, in the depressions surrounding the BTD and in some deep craters in Cthulhu (e.g. Elliot crater, where evidences of polygonal cells may be supportive of a thick deposit), and suggests that these deposits may be stable over several Myrs. Second, a 10-20 m-thick mid-latitudinal band (30-45°N) of N_2 ice forms in most of our simulations and remains over several Myrs, which is consistent with observations (see Fig. 15 in Schmitt et al., 2017; Protopapa et al., 2017). The extent of such N_2 ice deposits toward lower latitudes is limited by the presence of tholin-covered regions, which tend to darken the surrounding areas thus preventing further accumulation of volatile ice.

All N_2 ice deposits are balanced by the main reservoir in Sputnik Planitia: as they form, the reservoir and therefore the surface level of N_2 ice within the basin decreases which reinforces the N_2 condensation in the basin (Bertrand and Forget, 2016), thus limiting the amount of N_2 ice that can form elsewhere. We also note that CH_4-rich ice on Pluto may not be trapped and buried by very large N_2-rich deposits, since N_2 ice is twice as dense as that of CH_4 and may sink through the CH_4 ice. For instance, on Triton, the Cantaloupe terrain may result from such a process (Schenk and Jackson, 1993).

5.1.3 The mid-to-polar N_2 and CH_4 deposits

At the north pole, New Horizons detected CH_4-rich deposits (Grundy et al., 2016; Schmitt et al., 2017; Protopapa et al., 2017). Most of our simulations reproduce this trend by predicting a seasonal (mm-thick) CH_4 ice deposit exposed on Pluto's surface at the north pole in 2015 (e.g. Figure 5,Figure 11), quickly disapearing and revealing the dark volatile-free surface during the following years. However, such a thin deposit should have allowed the spectrometers on-board New Horizons for the detection of the water ice bedrock below. The fact that water ice has not been detected anywhere in the polar region strongly suggests that at least several centimeters or even meters of CH_4-rich ice cover this region (or else the water ice is buried under photolytic byproducts).

Simulations #TI888_030_072 and #TI888_050_080 (Figure 6 and Figure 8 respectively) show that such perennial CH_4-rich deposits can be obtained at the poles, by assuming a very dark albedo for the BTD or a very bright albedo

for the polar CH_4 deposits. These results may be related to the yellow aspect of the polar region in false-color images (Olkin et al., 2017). For instance, the color may be due to the presence of tholins mixed with (or seen through) the thin CH_4-rich frost (Grundy et al., 2018). Alternatively, the polar reservoir of CH_4 may be perennial and have accumulated tholins over the last Myrs. The higher concentration of tholins in these deposits may be responsible for their peculiar color.

At northern mid-latitudes, we obtain the formation of N_2 ice deposits (on the bright CH_4 deposits), which tend to be seasonal above 37°N as they sublime from the poles during end spring/summer. This result explains the mid-latitudinal band of N_2-rich ice observed in 2015 (Protopapa et al., 2017; Schmitt et al., 2017), and is consistent with the latitudinal distribution of the different ice mixtures observed at these latitudes, indicative of N_2:CO sublimation processes (Protopapa et al., 2017; Schmitt et al., 2017). Our results predict that N_2 ice sublimation will continue during northern spring/summer (with a sublimation front advancing southward, as suggested in Protopapa et al. (2017)) and reveal more CH_4-rich terrains, while the redeposition of N_2 ice will occur in the southern winter hemisphere. Note that N_2 ice is always more stable in the depressions than outside, which explains the patchy distribution of N_2 found at northern mid-latitudes (see Fig. 15 in Schmitt et al., 2017).

In the model, the seasonal mid-latitudinal N_2 ice deposits are able to trap large amounts of CH_4 ice, provided that a constant source is present elsewhere (in this case, the BTD). This also occurs in simulations performed at other epochs (t_0=-100, -200, -300 Myrs) and explains the thick mantle of ice observed by New Horizons at these latitudes.

In the model, the N_2 ice deposits forming between 30°N-37°N tend to be perennial, because they are located in colder regions on average over several Myrs (this is an effect of subsurface thermal inertia, as shown by Fig. 4.b in B2018). At lower latitudes, the dark albedo of the equatorial volatile-free surface prevent further N_2 condensation. However, thin CH_4 frosts may form on these dark terrains during winter (see e.g Figure 11). This is consistent with the third latitudinal band observed on Pluto and mentioned in Protopapa et al. (2017), where CH_4-rich deposits are observed between 20°N-30°N (also shown in Earle et al., 2018b). At these latitudes, which border the dark tholin-covered regions, N_2 ice deposits are not stable due to the darker albedo and the high rate of contamination and darkening by tholins. However, CH_4-rich frosts may form and last until spring/summer or even last longer and form perennial deposits.

Note that the exact latitudes where the volatile ice deposits form in the model are sensitive to the surface properties (albedo, emissivity, thermal inertia).

In addition, dilution and mixing processes of these ices should impact their latitudinal distribution.

5.1.4 Best case simulations

A simulation that best matches Pluto's observation would show (1) an ice distribution in 2015 as observed by New Horizons, that is with CH_4 ice exposed at the north pole and N_2 ice subliming at mid-latitudes, (2) a peak surface pressure occurring after 2015, and (3) an atmospheric mixing ratio for CH_4 around 0.5% in the period 2010-2015 (Lellouch et al., 2011a, 2015). In this paper, although we explored many cases and obtained a plethora of results, it is difficult to find one simulation that reconciles all these observations. Generally speaking, simulations performed with a thermal inertia for water ice of 400 SI give the best results. This thermal inertia is low compared to the estimations (Leyrat et al., 2016) but allows for thicker deposits of CH_4 at the poles, which is consistent with the observations.

5.2 Scenario for the formation of observed CH_4-rich and N_2-rich reservoirs

We have identified two perennial reservoirs of volatile ice on Pluto which add to Sputnik Planitia, as shown in Figure 18: the mid-latitudinal regions (mantle of CH_4 ice and meter-thick N_2 ice deposits) and the equatorial regions east of Sputnik Planitia (BTD of CH_4 ice and low-altitude N_2 ice deposits).

Our model is able to reproduce the formation of the equatorial and mid-latitudinal perennial CH_4 reservoirs, although not at the same time. Indeed, both the BTD and the mid-latitudinal CH_4 mantle need a source of available CH_4 ice to form, and in our simulations one reservoir dominates the other, depending on the assumed CH_4 albedo. This suggests a complex history for the formation of these perennial reservoirs.

The reservoir in Sputnik Planitia must have been the first to form, since the basin is the oldest geologic feature identified on Pluto (Moore et al., 2016, > 4 billion years), and since its infilling with all available surface N_2 ice has been modeled and estimated to be complete by tens of millions of years following its formation (Bertrand et al., 2018).

We could imagine that at a time in Pluto's history, large CH_4-rich ice deposits formed at the equator. At first, they may have been covered by N_2-rich ice deposits, but as they thickened up and reached higher altitudes with time, N_2-rich ice probably became less stable on these deposits and remained in depressions only. The high-altitude CH_4 ice deposits may have then become older and darker with time, forming a plateau of darkened CH_4-rich, precursor

to the BTD. In our simulations, we show that there is a net transport of CH_4 ice from the BTD to the mid-latitudes, suggesting that the thick mantle of CH_4 ice is subsequent to the BTD, which could have formed by erosionnal sublimation. Consequently, if the BTD formed very early in Pluto's history, why have they not entirely disappeared by now? One solution is that the current BTD formed only recently in Pluto's history, and may be currently disappearing. One could imagine that the astronomical cycles of Pluto may have changed over the last billion years and created the conditions for the BTD only recently. However, Pluto is thought to be subject to very little perturbations (Dobrovolskis et al., 1997) and the presence of non-eroded ancient craters at the equator demonstrates a certain stability of the astronomical cycles (Binzel et al., 2017). Another solution is that a long-term cycle exists between the perennial reservoirs, as illustrated by the black arrows on Figure 18. In this case, processes not taken into account in our model must exist and refill Pluto's system with CH_4 gas and ice.

For instance, large amounts of CH_4 could be released at the northern and southern edges of the Sputnik Planitia ice sheet during the high obliquity periods, where intense N_2 sublimation occurs (Bertrand et al., 2018). In fact, New Horizons observations of the northern edge of the ice sheet revealed very dark plains of N_2-rich ice enriched in CH_4 ice (1-2%, compared to 0.3% in the rest of the ice sheet), which supports this scenario (Protopapa et al., 2017).

Albedo and topography run-away variations may also play a significant role in redistributing N_2 and CH_4 ice to different reservoirs (Earle et al., 2018a), as well as changes in ice composition, saturation, contamination or irradiation (Schmitt et al., 2017; Protopapa et al., 2017; Grundy et al., 2018). Another possibility is the re-supply of large amounts of CH_4 from Pluto's interior, where sources of CH_4 clathrate could be stored and released over time via outgassing or cryovolcanism, as proposed on Titan (Lunine and Atreya, 2008; Moore et al., 2016).

The lack of knowledge about these mechanisms makes it difficult to infer the total CH_4 inventory in the system. A lower limit could be estimated by assuming that the high latitudes are only covered by thin layers of CH_4 ice and that most of the CH_4 reservoir is contained in the Bladed Terrain Deposits (the contribution of 0.3-0.5% of CH_4 in the N_2 reservoir of Sputnik Planitia is negligible). Such a reservoir has been estimated to 22 m on global average in Section 2.4, for 500 m thick BTD, but could be raised to 100 m if we assume 2-2.5 km thick BTD. An upper limit of 1 km could be estimated by considering the BTD and a 1-km thick CH_4 mantle at latitudes higher than $15°$ (740 m on global average). Note that the weak escape rate of CH_4 observed by New Horizons suggests that the reservoir of CH_4 changed by only 28 m over the age of the solar system (Gladstone et al., 2016).
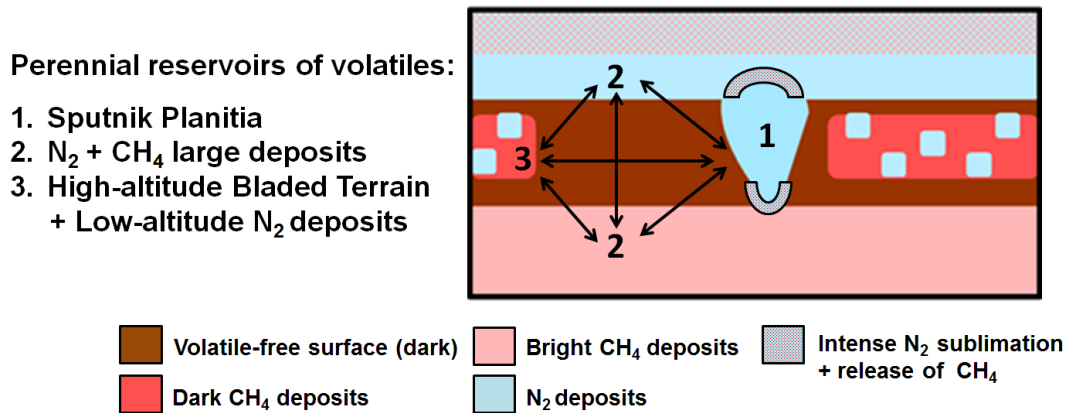
Fig. 18. The perennial reservoirs of N_2 and CH_4 ice identified on Pluto. The black arrows represent the possible exchanges of volatile ice that may occur over timescales of millions of years.

6 Conclusions

The Pluto volatile transport model has been used to simulate the evolution of large N_2 and CH_4 ice reservoirs over seasonal and astronomical timescales, in response to the Milankovitch paleoclimate cycles. This complements the work done by B2018, which only explored the cycles of N_2.

Our simulations reproduce the formation of massive perennial deposits of CH_4-rich ice at the equator, explaining the observation of the Bladed Terrain Deposits at these locations. The configuration of Pluto's orbit and obliquity is responsible for the small but detectable asymmetry of these terrains around the equator, which form further in the north than in the south, as seen in our model.

We demonstrate that high CH_4 ice albedo values may sufficiently cool the surface and trigger N_2 condensation which then cold traps more CH_4 ice. We obtained a plethora of results depending on the assumed albedo for CH_4 ice, which controls the perennial or seasonal nature of the deposits. Assuming relatively dark Bladed Terrain Deposits allows the formation of perennial N_2 ice in the depressions of these terrains only, which is consistent with the observations. Assuming relatively bright mid-to-polar CH_4 ice deposits leads to the formation of up to 10-m thick N_2 deposits on the CH_4 ice deposits, in particular at low elevations. During northern spring and summer, these N_2 deposits sublime from the pole, explaining the latitudinal distribution of N_2-rich and CH_4-rich ices observed by New Horizons in 2015 at the mid-northern latitudes (Protopapa et al., 2017; Schmitt et al., 2017).

At the north pole, the disapearance of CH_4-rich frost during the next decade predicted by most of our simulation may not happen because the observations

39

suggest larger deposits than those simulated. However, this is a testable prediction, as well as the removal of N_2-rich ice from the northern high latitudes, since it should result in changes in Pluto's spectrum and maybe albedo and color, observable from Earth.

Our simulations also show that a large amount of CH_4 ice can accumulate in the mid-latitudes due to the cold-trap effect of N_2 ice, forming a thick mantle consistent with the observations of Pluto's surface by New Horizons. In the model, CH_4 ice is moved from the Bladed Terrain Deposits, which tends to disappear as the mid-latitude mantle forms.

These simulations indicate that there is always enough gaseous CH_4 in Pluto's atmosphere for it to remain relatively opaque at Lyman-α wavelengths over astronomical cycles, in particular during high-to-moderate obliquity periods. However, the small amounts of Lyman-α flux reaching the surface can be significant to the surface chemistry.

Finally, our results highlight the strong coupling between the CH_4 and the N_2 cycle and the role of CH_4 material as a controlling agent of this coupling. They suggest a complex history for Pluto's perennial reservoirs as large amounts of CH_4 ice may have been exchanged between Sputnik Planitia, the Bladed Terrain, and the mid-latitudes, over timescales of hundreds of million years. The evolution of these reservoirs may be driven by positive ("run-away") or negative feedbacks involving ice albedo, emissivity, dilution and mixing coefficient, contamination by haze particles, or ice irradiation. In order to improve our understanding of Pluto's surface, future versions of the Pluto volatile transport model should implement these processes and explore how they impact Pluto's climate.

References

T. Bertrand and F. Forget. 3D modeling of organic haze in Pluto's atmosphere. Icarus, 287:72–86, May 2017. doi: 10.1016/j.icarus.2017.01.016.

T. Bertrand and F. Forget. Observed glacier and volatile distribution on Pluto from atmospheretopography processes. *Nature*, 987, December 2016. doi: 10.1038/nature19337.

T. Bertrand, F. Forget, O. M. Umurhan, W. M. Grundy, B. Schmitt, S. Protopapa, A. M. Zangari, O. L. White, P. M. Schenk, K. N. Singer, A. Stern, H. A. Weaver, L. A. Young, K. Ennico, and C. B. Olkin. The nitrogen cycles on Pluto over seasonal and astronomical timescales. Icarus, 309:277–296, July 2018. doi: 10.1016/j.icarus.2018.03.012.

R. P. Binzel, A. M. Earle, M. W. Buie, L. A. Young, S. A. Stern, C. B. Olkin, K. Ennico, J. M. Moore, W. Grundy, H. A. Weaver, C. M. Lisse, and T. R. Lauer. Climate zones on Pluto and Charon. *Icarus*, 287:30–36, May 2017. doi: 10.1016/j.icarus.2016.07.023.

B. J. Buratti, J. D. Hofgartner, M. D. Hicks, H. A. Weaver, S. A. Stern, T. Momary, J. A. Mosher, R. A. Beyer, A. J. Verbiscer, A. M. Zangari, L. A. Young, C. M. Lisse, K. Singer, A. Cheng, W. Grundy, K. Ennico, and C. B. Olkin. Global albedos of Pluto and Charon from LORRI New Horizons observations. *Icarus*, 287:207–217, May 2017. doi: 10.1016/j.icarus.2016.11. 012.

A. R. Dobrovolskis, S. J. Peale, and A. W. Harris. *Dynamics of the Pluto-Charon Binary. In: S.A. Stern, D.J. Tholen (Eds.), Pluto and Charon, University of Arizona Press, Tucson, 159-190*. 1997.

A. M. Earle, R. P. Binzel, L. A. Young, S. A. Stern, K. Ennico, W. Grundy, C. B. Olkin, and H. A. Weaver. Long-term surface temperature modeling of Pluto. *Icarus*, 287:37–46, May 2017. doi: 10.1016/j.icarus.2016.09.036.

A. M. Earle, R. P. Binzel, L. A. Young, S. A. Stern, K. Ennico, W. Grundy, C. B. Olkin, H. A. Weaver, and New Horizons Surface Composition Theme. Albedo matters: Understanding runaway albedo variations on Pluto. *Icarus*, 303:1–9, March 2018a. doi: 10.1016/j.icarus.2017.12.015.

A. M. Earle, W. Grundy, C. J. A. Howett, C. B. Olkin, A. H. Parker, F. Scipioni, R. P. Binzel, R. A. Beyer, J. C. Cook, D. P. Cruikshank, C. M. Dalle Ore, K. Ennico, S. Protopapa, D. C. Reuter, P. M. Schenk, B. Schmitt, S. A. Stern, H. A. Weaver, L. A. Young, and New Horizons Surface Composition Theme Team. Methane distribution on Pluto as mapped by the New Horizons Ralph/MVIC instrument. *Icarus*, 314:195–209, November 2018b. doi: 10.1016/j.icarus.2018.06.005.

J. Eluszkiewicz and D. J. Stevenson. Rheology of solid methane and nitrogen - Applications of Triton. Geophys. Res. Lett., 17:1753–1756, September 1990. doi: 10.1029/GL017i010p01753.

F. Forget, T. Bertrand, M. Vangvichith, J. Leconte, E. Millour, and E. Lellouch. A post-new horizons global climate model of Pluto including the N_2, CH_4 and CO cycles. *Icarus*, 287:54–71, May 2017. doi: 10.1016/j.icarus.

2016.11.038.

G. Gladstone, W. R. Pryor, and S. Alan Stern. Ly α @Pluto. *Icarus*, 246: 279–284, January 2015. doi: 10.1016/j.icarus.2014.04.016.

G. R. Gladstone, S. A. Stern, K. Ennico, C. B. Olkin, H. A. Weaver, L. A. Young, M. E. Summers, D. F. Strobel, D. P. Hinson, J. A. Kammer, A. H. Parker, A. J. Steffl, I. R. Linscott, J. W. Parker, A. F. Cheng, D. C. Slater, M. H. Versteeg, T. K. Greathouse, K. D. Retherford, H. Throop, N. J. Cunningham, W. W. Woods, K. N. Singer, C. C. C. Tsang, E. Schindhelm, C. M. Lisse, M. L. Wong, Y. L. Yung, X. Zhu, W. Curdt, P. Lavvas, E. F. Young, G. L. Tyler, F. Bagenal, W. M. Grundy, W. B. McKinnon, J. M. Moore, J. R. Spencer, T. Andert, J. Andrews, M. Banks, B. Bauer, J. Bauman, O. S. Barnouin, P. Bedini, K. Beisser, R. A. Beyer, S. Bhaskaran, R. P. Binzel, E. Birath, M. Bird, D. J. Bogan, A. Bowman, V. J. Bray, M. Brozovic, C. Bryan, M. R. Buckley, M. W. Buie, B. J. Buratti, S. S. Bushman, A. Calloway, B. Carcich, S. Conard, C. A. Conrad, J. C. Cook, D. P. Cruikshank, O. S. Custodio, C. M. D. Ore, C. Deboy, Z. J. B. Dischner, P. Dumont, A. M. Earle, H. A. Elliott, J. Ercol, C. M. Ernst, T. Finley, S. H. Flanigan, G. Fountain, M. J. Freeze, J. L. Green, Y. Guo, M. Hahn, D. P. Hamilton, S. A. Hamilton, J. Hanley, A. Harch, H. M. Hart, C. B. Hersman, A. Hill, M. E. Hill, M. E. Holdridge, M. Horanyi, A. D. Howard, C. J. A. Howett, C. Jackman, R. A. Jacobson, D. E. Jennings, H. K. Kang, D. E. Kaufmann, P. Kollmann, S. M. Krimigis, D. Kusnierkiewicz, T. R. Lauer, J. E. Lee, K. L. Lindstrom, A. W. Lunsford, V. A. Mallder, N. Martin, D. J. McComas, R. L. McNutt, D. Mehoke, T. Mehoke, E. D. Melin, M. Mutchler, D. Nelson, F. Nimmo, J. I. Nunez, A. Ocampo, W. M. Owen, M. Paetzold, B. Page, F. Pelletier, J. Peterson, N. Pinkine, M. Piquette, S. B. Porter, S. Protopapa, J. Redfern, H. J. Reitsema, D. C. Reuter, J. H. Roberts, S. J. Robbins, G. Rogers, D. Rose, K. Runyon, M. G. Ryschkewitsch, P. Schenk, B. Sepan, M. R. Showalter, M. Soluri, D. Stanbridge, T. Stryk, J. R. Szalay, M. Tapley, A. Taylor, H. Taylor, O. M. Umurhan, A. J. Verbiscer, M. H. Versteeg, M. Vincent, R. Webbert, S. Weidner, G. E. Weigle, O. L. White, K. Whittenburg, B. G. Williams, K. Williams, S. Williams, A. M. Zangari, and E. Zirnstein. The atmosphere of Pluto as observed by New Horizons. *Science*, 351:aad8866, March 2016. doi: 10.1126/science.aad8866.

W. M. Grundy and M. W. Buie. Distribution and Evolution of CH4, N2, and CO Ices on Pluto's Surface: 1995 to 1998. *Icarus*, 153:248–263, October 2001. doi: 10.1006/icar.2001.6684.

W. M. Grundy, C. B. Olkin, L. A. Young, M. W. Buie, and E. F. Young. Near-infrared spectral monitoring of Pluto's ices: Spatial distribution and secular evolution. *Icarus*, 223:710–721, April 2013. doi: 10.1016/j.icarus.2013.01.019.

W. M. Grundy, R. P. Binzel, B. J. Buratti, J. C. Cook, D. P. Cruikshank, C. M. Dalle Ore, A. M. Earle, K. Ennico, C. J. A. Howett, A. W. Lunsford, C. B. Olkin, A. H. Parker, S. Philippe, S. Protopapa, E. Quirico, D. C. Reuter, B. Schmitt, K. N. Singer, A. J. Verbiscer, R. A. Beyer, M. W. Buie,

A. F. Cheng, D. E. Jennings, I. R. Linscott, J. W. Parker, P. M. Schenk, J. R. Spencer, J. A. Stansberry, S. A. Stern, H. B. Throop, C. C. C. Tsang, H. A. Weaver, G. E. Weigle, and L. A. Young. Surface compositions across Pluto and Charon. *Science*, 351:aad9189, March 2016. doi: 10.1126/science. aad9189.

W. M. Grundy, T. Bertrand, R. P. Binzel, M. W. Buie, B. J. Buratti, A. F. Cheng, J. C. Cook, D. P. Cruikshank, S. L. Devins, C. M. Dalle Ore, A. M. Earle, K. Ennico, F. Forget, P. Gao, G. R. Gladstone, C. J. A. Howett, D. E. Jennings, J. A. Kammer, T. R. Lauer, I. R. Linscott, C. M. Lisse, A. W. Lunsford, W. B. McKinnon, C. B. Olkin, A. H. Parker, S. Protopapa, E. Quirico, D. C. Reuter, B. Schmitt, K. N. Singer, J. A. Spencer, S. A. Stern, D. F. Strobel, M. E. Summers, H. A. Weaver, G. E. Weigle, M. L. Wong, E. F. Young, L. A. Young, and X. Zhang. Pluto's haze as a surface material. *Icarus*, 314:232–245, November 2018. doi: 10.1016/j.icarus.2018. 05.019.

C. J. Hansen and D. A. Paige. Seasonal Nitrogen Cycles on Pluto. *Icarus*, 120:247–265, April 1996. doi: 10.1006/icar.1996.0049.

C. J. Hansen, D. A. Paige, and L. A. Young. Pluto's climate modeled with new observational constraints. *Icarus*, 246:183–191, January 2015. doi: 10.1016/j.icarus.2014.03.014.

A. D. Howard, J. M. Moore, O. M. Umurhan, O. L. White, R. S. Anderson, W. B. McKinnon, J. R. Spencer, P. M. Schenk, R. A. Beyer, S. A. Stern, K. Ennico, C. B. Olkin, H. A. Weaver, and L. A. Young. Present and past glaciation on Pluto. *Icarus*, 287:287–300, May 2017. doi: 10.1016/j.icarus. 2016.07.006.

E. Lellouch, C. de Bergh, B. Sicardy, H. U. Käufl, and A. Smette. High resolution spectroscopy of Pluto's atmosphere: detection of the 2.3 μm CH_4 bands and evidence for carbon monoxide. *Astronomy&Astroph.*, 530:L4, June 2011a. doi: 10.1051/0004-6361/201116954.

E. Lellouch, J. Stansberry, J. Emery, W. Grundy, and D. P. Cruikshank. Thermal properties of Pluto's and Charon's surfaces from Spitzer observations. *Icarus*, 214:701–716, August 2011b. doi: 10.1016/j.icarus.2011.05.035.

E. Lellouch, C. de Bergh, B. Sicardy, F. Forget, M. Vangvichith, and H.-U. Käufl. Exploring the spatial, temporal, and vertical distribution of methane in Pluto's atmosphere. *Icarus*, 246:268–278, January 2015. doi: 10.1016/j. icarus.2014.03.027.

C. Leyrat, R. D. Lorenz, and A. Le Gall. Probing Pluto's underworld: Ice temperatures from microwave radiometry decoupled from surface conditions. *Icarus*, 268:50–55, April 2016. doi: 10.1016/j.icarus.2015.12.016.

J. Lunine and S. Atreya. The methane cycle on Titan. *Nature Geoscience*, 1: 335, May 2008. doi: 10.1038/ngeo187.

C. K. Materese, D. P. Cruikshank, S. A. Sandford, H. Imanaka, and M. Nuevo. Ice Chemistry on Outer Solar System Bodies: Electron Radiolysis of N2-, CH4-, and CO-Containing Ices. *Astrophys. J.*, 812:150, October 2015. doi: 10.1088/0004-637X/812/2/150.

F. Merlin. New constraints on the surface of Pluto. *Astronomy&Astroph.*, 582:A39, October 2015. doi: 10.1051/0004-6361/201526721.

J. M. Moore, W. B. McKinnon, J. R. Spencer, A. D. Howard, P. M. Schenk, R. A. Beyer, F. Nimmo, K. N. Singer, O. M. Umurhan, O. L. White, S. A. Stern, K. Ennico, C. B. Olkin, H. A. Weaver, L. A. Young, R. P. Binzel, M. W. Buie, B. J. Buratti, A. F. Cheng, D. P. Cruikshank, W. M. Grundy, I. R. Linscott, H. J. Reitsema, D. C. Reuter, M. R. Showalter, V. J. Bray, C. L. Chavez, C. J. A. Howett, T. R. Lauer, C. M. Lisse, A. H. Parker, S. B. Porter, S. J. Robbins, K. Runyon, T. Stryk, H. B. Throop, C. C. C. Tsang, A. J. Verbiscer, A. M. Zangari, A. L. Chaikin, D. E. Wilhelms, F. Bagenal, G. R. Gladstone, T. Andert, J. Andrews, M. Banks, B. Bauer, J. Bauman, O. S. Barnouin, P. Bedini, K. Beisser, S. Bhaskaran, E. Birath, M. Bird, D. J. Bogan, A. Bowman, M. Brozovic, C. Bryan, M. R. Buckley, S. S. Bushman, A. Calloway, B. Carcich, S. Conard, C. A. Conrad, J. C. Cook, O. S. Custodio, C. M. D. Ore, C. Deboy, Z. J. B. Dischner, P. Dumont, A. M. Earle, H. A. Elliott, J. Ercol, C. M. Ernst, T. Finley, S. H. Flanigan, G. Fountain, M. J. Freeze, T. Greathouse, J. L. Green, Y. Guo, M. Hahn, D. P. Hamilton, S. A. Hamilton, J. Hanley, A. Harch, H. M. Hart, C. B. Hersman, A. Hill, M. E. Hill, D. P. Hinson, M. E. Holdridge, M. Horanyi, C. Jackman, R. A. Jacobson, D. E. Jennings, J. A. Kammer, H. K. Kang, D. E. Kaufmann, P. Kollmann, S. M. Krimigis, D. Kusnierkiewicz, J. E. Lee, K. L. Lindstrom, A. W. Lunsford, V. A. Mallder, N. Martin, D. J. McComas, R. L. McNutt, D. Mehoke, T. Mehoke, E. D. Melin, M. Mutchler, D. Nelson, J. I. Nunez, A. Ocampo, W. M. Owen, M. Paetzold, B. Page, J. W. Parker, F. Pelletier, J. Peterson, N. Pinkine, M. Piquette, S. Protopapa, J. Redfern, J. H. Roberts, G. Rogers, D. Rose, K. D. Retherford, M. G. Ryschkewitsch, E. Schindhelm, B. Sepan, M. Soluri, D. Stanbridge, A. J. Steffl, D. F. Strobel, M. E. Summers, J. R. Szalay, M. Tapley, A. Taylor, H. Taylor, G. L. Tyler, M. H. Versteeg, M. Vincent, R. Webbert, S. Weidner, G. E. Weigle, K. Whittenburg, B. G. Williams, K. Williams, S. Williams, W. W. Woods, and E. Zirnstein. The geology of Pluto and Charon through the eyes of New Horizons. *Science*, 351:1284–1293, March 2016. doi: 10.1126/science.aad7055.

J. M. Moore, A. D. Howard, O. M. Umurhan, O. L. White, P. M. Schenk, R. A. Beyer, W. B. McKinnon, J. R. Spencer, W. M. Grundy, T. R. Lauer, F. Nimmo, L. A. Young, S. A. Stern, H. A. Weaver, C. B. Olkin, and K. Ennico. Sublimation as a landform-shaping process on Pluto. *Icarus*, 287: 320–333, May 2017. doi: 10.1016/j.icarus.2016.08.025.

J. M. Moore, A. D. Howard, O. M. Umurhan, O. L. White, P. M. Schenk, R. A. Beyer, W. B. McKinnon, J. R. Spencer, K. N. Singer, W. M. Grundy, A. M. Earle, B. Schmitt, S. Protopapa, F. Nimmo, D. P. Cruikshank, D. P. Hinson, L. A. Young, S. A. Stern, H. A. Weaver, C. B. Olkin, K. Ennico, G. Collins, T. Bertrand, F. Forget, F. Scipioni, and New Horizons Science Team. Bladed Terrain on Pluto: Possible origins and evolution. *Icarus*, 300: 129–144, January 2018. doi: 10.1016/j.icarus.2017.08.031.

J. E. Moores, C. L. Smith, A. D. Toigo, and S. D. Guzewich. Penitentes as the origin of the bladed terrain of Tartarus Dorsa on Pluto. *Nature*, 541: 188–190, January 2017. doi: 10.1038/nature20779.

C. B. Olkin, L. A. Young, D. Borncamp, A. Pickles, B. Sicardy, M. Assafin, F. B. Bianco, M. W. Buie, A. D. de Oliveira, M. Gillon, R. G. French, A. Ramos Gomes, E. Jehin, N. Morales, C. Opitom, J. L. Ortiz, A. Maury, M. Norbury, F. Braga-Ribas, R. Smith, L. H. Wasserman, E. F. Young, M. Zacharias, and N. Zacharias. Evidence that Pluto's atmosphere does not collapse from occultations including the 2013 May 04 event. *Icarus*, 246:220–225, January 2015. doi: 10.1016/j.icarus.2014.03.026.

C. B. Olkin, J. R. Spencer, W. M. Grundy, A. H. Parker, R. A. Beyer, P. M. Schenk, C. J. A. Howett, S. A. Stern, D. C. Reuter, H. A. Weaver, L. A. Young, K. Ennico, R. P. Binzel, M. W. Buie, J. C. Cook, D. P. Cruikshank, C. M. Dalle Ore, A. M. Earle, D. E. Jennings, K. N. Singer, I. E. Linscott, A. W. Lunsford, S. Protopapa, B. Schmitt, E. Weigle, and the New Horizons Science Team. The Global Color of Pluto from New Horizons. AJ, 154:258, December 2017. doi: 10.3847/1538-3881/aa965b.

S. Protopapa, W. M. Grundy, D. C. Reuter, D. P. Hamilton, C. M. Dalle Ore, J. C. Cook, D. P. Cruikshank, B. Schmitt, S. Philippe, E. Quirico, R. P. Binzel, A. M. Earle, K. Ennico, C. J. A. Howett, A. W. Lunsford, C. B. Olkin, A. Parker, K. N. Singer, A. Stern, A. J. Verbiscer, H. A. Weaver, and L. A. Young. Pluto's global surface composition through pixel-by-pixel Hapke modeling of New Horizons Ralph/LEISA data. *Icarus*, 287:218–228, May 2017. doi: 10.1016/j.icarus.2016.11.028.

P. Schenk and M. P. A. Jackson. Diapirism on Triton - A record of crustal layering and instability. *Geology*, 21:299–302, April 1993. doi: 10.1130/0091-7613(1993)021⟨0299:DOTARO⟩2.3.CO;2.

B. Schmitt, S. Philippe, W. M. Grundy, D. C. Reuter, R. Cote, E. Quirico, S. Protopapa, L. A. Young, R. P. Binzel, J. C. Cook, D. P. Cruikshank, C. M. Dalle Ore, A. M. Earle, K. Ennico, C. J. A. Howett, D. E. Jennings, I. R. Linscott, A. W. Lunsford, C. B. Olkin, A. H. Parker, J. W. Parker, K. N. Singer, J. R. Spencer, J. A. Stansberry, S. A. Stern, C. C. C. Tsang, A. J. Verbiscer, and H. A. Weaver. Physical state and distribution of materials at the surface of Pluto from New Horizons LEISA imaging spectrometer. *Icarus*, 287:229–260, May 2017. doi: 10.1016/j.icarus.2016.12.025.

J. R. Spencer, J. A. Stansberry, L. M. Trafton, E. F. Young, R. P. Binzel, and S. K. Croft. Volatile Transport, Seasonal Cycles, and Atmospheric Dynamics on Pluto. In S. A. Stern and D. J. Tholen, editors, *Pluto and Charon*, page 435, 1997.

J. A. Stansberry and R. V. Yelle. Emissivity and the Fate of Pluto's Atmosphere. *Icarus*, 141:299–306, October 1999. doi: 10.1006/icar.1999.6169.

S. A. Stern, F. Bagenal, K. Ennico, G. R. Gladstone, W. M. Grundy, W. B. McKinnon, J. M. Moore, C. B. Olkin, J. R. Spencer, H. A. Weaver, L. A. Young, T. Andert, J. Andrews, M. Banks, B. Bauer, J. Bauman, O. S. Barnouin, P. Bedini, K. Beisser, R. A. Beyer, S. Bhaskaran, R. P. Binzel,

E. Birath, M. Bird, D. J. Bogan, A. Bowman, V. J. Bray, M. Brozovic, C. Bryan, M. R. Buckley, M. W. Buie, B. J. Buratti, S. S. Bushman, A. Calloway, B. Carcich, A. F. Cheng, S. Conard, C. A. Conrad, J. C. Cook, D. P. Cruikshank, O. S. Custodio, C. M. Dalle Ore, C. Deboy, Z. J. B. Dischner, P. Dumont, A. M. Earle, H. A. Elliott, J. Ercol, C. M. Ernst, T. Finley, S. H. Flanigan, G. Fountain, M. J. Freeze, T. Greathouse, J. L. Green, Y. Guo, M. Hahn, D. P. Hamilton, S. A. Hamilton, J. Hanley, A. Harch, H. M. Hart, C. B. Hersman, A. Hill, M. E. Hill, D. P. Hinson, M. E. Holdridge, M. Horanyi, A. D. Howard, C. J. A. Howett, C. Jackman, R. A. Jacobson, D. E. Jennings, J. A. Kammer, H. K. Kang, D. E. Kaufmann, P. Kollmann, S. M. Krimigis, D. Kusnierkiewicz, T. R. Lauer, J. E. Lee, K. L. Lindstrom, I. R. Linscott, C. M. Lisse, A. W. Lunsford, V. A. Mallder, N. Martin, D. J. McComas, R. L. McNutt, D. Mehoke, T. Mehoke, E. D. Melin, M. Mutchler, D. Nelson, F. Nimmo, J. I. Nunez, A. Ocampo, W. M. Owen, M. Paetzold, B. Page, A. H. Parker, J. W. Parker, F. Pelletier, J. Peterson, N. Pinkine, M. Piquette, S. B. Porter, S. Protopapa, J. Redfern, H. J. Reitsema, D. C. Reuter, J. H. Roberts, S. J. Robbins, G. Rogers, D. Rose, K. Runyon, K. D. Retherford, M. G. Ryschkewitsch, P. Schenk, E. Schindhelm, B. Sepan, M. R. Showalter, K. N. Singer, M. Soluri, D. Stanbridge, A. J. Steffl, D. F. Strobel, T. Stryk, M. E. Summers, J. R. Szalay, M. Tapley, A. Taylor, H. Taylor, H. B. Throop, C. C. C. Tsang, G. L. Tyler, O. M. Umurhan, A. J. Verbiscer, M. H. Versteeg, M. Vincent, R. Webbert, S. Weidner, G. E. Weigle, O. L. White, K. Whittenburg, B. G. Williams, K. Williams, S. Williams, W. W. Woods, A. M. Zangari, and E. Zirnstein. The Pluto system: Initial results from its exploration by New Horizons. *Science*, 350:aad1815, October 2015. doi: 10.1126/science.aad1815.

S. P. Tan and J. S. Kargel. Solid-phase equilibria on Pluto's surface. *MNRAS*, 474:4254–4263, March 2018. doi: 10.1093/mnras/stx3036.

A. D. Toigo, R. G. French, P. J. Gierasch, S. D. Guzewich, X. Zhu, and M. I. Richardson. General circulation models of the dynamics of Pluto's volatile transport on the eve of the New Horizons encounter. *Icarus*, 254:306–323, July 2015. doi: 10.1016/j.icarus.2015.03.034.

L. M. Trafton. On the state of methane and nitrogen ice on Pluto and Triton: Implications of the binary phase diagram. *Icarus*, 246:197–205, January 2015. doi: 10.1016/j.icarus.2014.05.022.

E. F. Young. *An Albedo Map and Frost Model of Pluto*. PhD thesis, MASSACHUSETTS INSTITUTE OF TECHNOLOGY., 1993.

L. A. Young. Pluto's Seasons: New Predictions for New Horizons. *Astrophys. J.l*, 766:L22, April 2013. doi: 10.1088/2041-8205/766/2/L22.

L.A. Young. Volatile transport on inhomogeneous surfaces: I - analytic expressions, with application to pluto's day. *Icarus*, 221:80–88, 2012.

Acknowledgements